Tectonomorphic evolution of Marie Byrd Land – Implications for Cenozoic rifting activity and onset of West Antarctic glaciation

Cornelia Spiegel[1*], Julia Lindow[1], Peter J.J. Kamp[2], Ove Meisel[1], Samuel Mukasa[3], Frank Lisker[1], Gerhard Kuhn[4] Karsten Gohl[4]

1: University of Bremen, Department of Geosciences, Postbox 330 440, 28334 Bremen, Germany

2: School of Science, University of Waikato, Hamilton 2001, New Zealand

3: University of New Hampshire, Department of Earth Sciences, 56 College Road, Durham, NH 03824, USA

4: Alfred-Wegener-Institut Helmholtz-Zentrum für Polar- und Meeresforschung, Am Alten Hafen 26, 27568 Bremerhaven, Germany

*corresponding author: phone: +49 421 218 65280

Fax: +49 421 218 65309

E-mail: spiegelc@uni-bremen.de

Abstract

The West Antarctic Rift System is one of the largest continental rifts on Earth. Because it is obscured by the West Antarctic Ice Sheet, its evolution is still poorly understood. Here we present the first low-temperature thermochronology data from eastern Marie Byrd Land, an area that stretches ~1000 km along the rift system, in order to shed light on its development. Furthermore, we petrographically analysed glacially transported detritus deposited in the marine realm, offshore Marie Byrd Land, to augment the data available from the limited terrestrial exposures. Our data provide information about the subglacial geology, and the tectonic and morphologic history of the rift system. Dominant lithologies of coastal Marie Byrd Land are igneous rocks that intruded (presumably early Paleozoic) low-grade meta-sedimentary rocks. No evidence was found for un-metamorphosed sedimentary rocks exposed beneath the ice. According to the thermochronology data, rifting occurred in two episodes. The earlier occurred between ~100 and 60 Ma and led to widespread tectonic denudation and block faulting over large areas of Marie Byrd Land. The later episode started during the Early Oligocene and was confined to western Pine Island Bay area. This Oligocene tectonic activity may be linked

kinematically to previously described rift structures reaching into Bellingshausen Sea and beneath Pine Island Glacier, all assumed to be of Cenozoic age. However, our data provide the first direct evidence for Cenozoic tectonic activity along the rift system outside the Ross Sea area. Furthermore, we tentatively suggest that uplift of the Marie Byrd Land dome only started at ~20 Ma; that is, nearly 10 Ma later than previously assumed. The Marie Byrd Land dome is the only extensive part of continental West Antarctica elevated above sea level. Since the formation of a continental ice sheet requires a significant area of emergent land, our data, although only based on few samples, imply that extensive glaciation of this part of West Antarctica may have only started since the early Miocene.

1 Introduction

The West Antarctic Rift System (WARS) transects the entire Antarctic continent. Its southern shoulder, formed by the Transantarctic Mountains, rises to more than 4500 m, while its bottom reaches down to ~2500 m below sea level along the deeply incised valleys of Bentley Subglacial Trench and the Byrd Subglacial Basin. Traces of the WARS separate several West Antarctic crustal blocks, including Marie Byrd Land, Thurston Island, Ellsworth-Whitmore Mountains, and Antarctic Peninsula (Daziel, 2006; Fig. 1). Tectonic activity within the WARS started during the Cretaceous and may have lasted through to the present. Unlike most other continental rifts that are better exposed, development of the WARS structure is poorly understood.

Unanswered questions remain about WARS concerning amounts of extension and crustal displacement, exact timing of rifting activity, positions of rift branches, the relationship between rifting and magmatism, and topographic evolution of the rift. For example, published amounts of total crustal extension range between 120 and 1800 km (DiVenere et al., 1994; Busetti et al., 1999; see Storti et al., 2008 for a more detailed discussion). While it is generally assumed (although not really proven) that the majority of crustal extension took place during the Cretaceous (e.g., Siddoway, 2008), about 180 km of Cenozoic crustal extension was proposed for the Ross Sea sector of the rift (Cande et al., 2000, Cande and Stock, 2004). However, while Cenozoic rifting is relatively well documented for

54 the Ross Sea area, no direct evidence for Cenozoic rift activity exists for the interior of Marie Byrd
55 Land (Dalziel, 2006). Also, it is still unknown how the WARS continues from the Ross Sea sector to
56 inner parts and other coastal areas of West Antarctica. On the basis of plate kinematic reconstructions
57 (Larter et al., 2002; Eagles et al., 2004), crustal thickness and geomorphic features, it has been
58 suggested that the WARS branches into the Amundsen Sea, following the trough beneath Pine Island
59 Glacier (Dalziel, 2006; Gohl et al., 2007; Jordan et al., 2010; Fig. 1); that it reaches into the
60 Bellingshausen Sea (Müller et al., 2007; Eagles et al., 2009; Bingham et al., 2012), or that it connects
61 the Ross Sea with the Weddell Sea (Dalziel, 2006). Another peculiar feature of the WARS is that
62 while most of the crustal extension is thought to have taken place during the Cretaceous, volcanic
63 activity mostly occurred during the late Cenozoic. The majority of volcanoes are situated in the area of
64 the Marie Byrd Land Dome, a large (~1000 x 500 km) domal structure rising to ~2700 m above sea
65 level (Fig. 1). Its uplift is thought to have started at ~29 to 25 Ma. This date is derived from the oldest
66 known volcanism from this area (Mt. Petras volcano), assuming that volcanic activity and uplift of the
67 dome were contemporaneous (Le Masurier, 2006). However, no direct evidence exists about the
68 timing of the exhumation of the Marie Byrd Land dome.

69 The reason for the many unknowns is that the WARS is overlain by the West Antarctic Ice Sheet,
70 which covers more than 98% of the outcrops. Presently, rapid thinning and retreat characterize the
71 West Antarctic Ice Sheet, particularly in the Amundsen Sea sector, and its glaciers show the highest
72 mass losses of ice across the entire Antarctic continent. The glacial cover hampers direct geological
73 investigations, but it also makes studying the WARS particularly interesting, since it provides insights
74 to interactions between lithospheric and glacial dynamics. In the first place, the basic reason for the
75 instability of the West Antarctic Ice Sheet is the tectonic setting of the underlying crust. Rifting and
76 associated crustal extension results in a subdued, low-lying topography, such that most of the West
77 Antarctic Ice Sheet is grounded below sea level (Fretwell et al., 2013). This, together with the inward
78 dipping bedrock (i.e., towards the continental interior) allows warm circumpolar deep water to
79 penetrate beneath the glaciers, melting them from below, causing grounding line retreat (Payne et al.,
80 2004, Jenkins et al., 2010; Ross et al., 2011). Deep-reaching rift valleys provide subglacial pathways
81 for warm ocean water, which is why their locations are of particular interest (Jordan et al., 2010;

Bingham et al., 2012). Furthermore, bedrock geology is an important parameter for glacial dynamics, influencing basal boundary conditions for ice movement. The nature of the bedrock "almost certainly plays a fundamental role in determining many large-scale dynamic aspects of ice-sheet behaviour" (Boulton, 2006). Also, tectonic evolution influences crustal heat flow and thus the thermal regime at the bases of glaciers (e.g., van der Veen et al., 2007). It also influences topography, which in turn is influenced by (glacial) erosion, illustrating interplay complexity. Topography provides important boundary conditions for the onset of continental glaciation. For West Antarctic Ice Sheet evolution, topographic evolution of Marie Byrd Land dome is particularly important, as it is the only large area of West Antarctica significantly elevated above sea level (excluding the Antarctic Peninsula). Continental glaciation of West Antarctica is assumed to have initiated either during late Paleogene or early Neogene (Barker et al., 2007; Wilson et al., 2013). At that time, the ocean temperatures were presumably too warm to allow for formation of a marine-based ice sheet, and for the formation of a terrestrially grounded ice sheet, a certain amount of topography above sea level was required (e.g., Wilson et al., 2013).

The aim of this paper is to (i) describe the bedrock geology exposed beneath the glacial cover of central Marie Byrd Land (Hobbs Coast area), (ii) outline the tectono-thermal history of the Amundsen Sea sector of the WARS (eastern Marie Byrd Land), particularly with respect to its Cenozoic rifting history and exhumation of the Marie Byrd Land dome. To achieve these goals, we provide petrographic descriptions of clasts from box cores retrieved from offshore Hobbs coast, as well as thermochronological data (fission track and apatite (U-Th-Sm)He analysis) derived from rock samples from both onshore and offshore Marie Byrd Land. Our data are the first low-temperature thermochronology data reported for eastern Marie Byrd Land.

2 Geological setting

2.1 Geological evolution of Marie Byrd Land

West Antarctica is composed of four major crustal blocks: Antarctic Peninsula, Ellsworth-Whitmore Mountains, Thurston Island, and Marie Byrd Land (Dalziel and Elliot, 1982; Fig. 1). On the basis of radiometric ages, Lopatin and Orlenko (1972) and Pankhurst et al. (1998) suggested that Marie Byrd Land originally comprised two realms; eastern Marie Byrd Land situated today along the Amundsen Sea, and western Marie Byrd Land, situated today adjacent to the Ross Sea. This study focuses on eastern Marie Byrd Land, comprising Hobbs Coast adjacent to Wrigley Gulf and Kohler Range and the Mt. Murphy area adjacent to the Amundsen Sea Embayment (Fig. 1).

Originally, West Antarctica was part of the active margin of Gondwana, with subduction of Phoenix plate/Proto-Pacific plate beneath it continuously or discontinuously since at least the Permian (Pankhurst et al., 1998; Mukasa and Dalziel, 2000; Larter et al., 2002). At that time, West Antarctica was still connected to Zealandia, comprising New Zealand, Campbell Plateau and Chatham Rise. Subduction led to the intrusion of calk-alkaline magmatic bodies. This batholitic belt, chiefly of Cretaceous age, forms most of the present-day coastal outcrops of Marie Byrd Land (Fig. 2, Table A1). Suduction ceased with the collision of the Hikurani Plateau with the Zealandia subduction margin at about 100 - 94 Ma (Mukasa and Dalziel, 2000). At ~90 Ma, intra-continental extension between East Antarctica and West Antarctica led to the opening of the WARS. Shortly thereafter, at ~83 Ma (Larter et al., 2002; Eagles et al., 2004; Gohl, 2012), West Antarctica separated from Zealandia. As pointed out by Siddoway (2008), the breakup between West Antarctica and Zealandia was apparently distinct from opening of the WARS as they had different structures (see also, Tessensohn and Wörner, 1991; Lawver and Gahagan, 1994; Sutherland, 1999).

During the Late Cretaceous, but prior to continental breakup, an erosion surface formed affecting ~90 Ma rocks on both the New Zealand and West Antarctic sides (LeMasurier and Landis, 1996). According to evidence from the New Zealand side, this erosion surface formed at low elevations close to sea level and was completed by ~75 Ma. This equivalent Cretaceous erosion surface across West Antarctica is the main "marker horizon" for correlations. It displays low relief <50 m, and, associated with the uplift of Marie Byrd Land dome, it is today elevated to 2700 m at the crest of the dome, and to 400 m at the margins.. Volcanism associated with the WARS started at 29 to 25 Ma and is thought

to have commenced contemporaneously with uplift of Marie Byrd Land dome (LeMasurier, 2008). Today, Marie Byrd Land shows one of the highest densities of volcanoes on Earth, the age of volcanic activity gradually decreasing from Oligocene ages at the crest to still active volcanism towards the margins of the dome (e.g. . Mt. Siple; Fig. 2). Despite the strong magmatic activity that may have resulted in crustal thickening, the dome rests on extended crust similar to the surrounding areas of the WARS, which is why it is assumed to be supported by a mantle plume (LeMasurier 2006).

2.2 Exposed bedrocks of eastern Marie Byrd Land

Rocks are mostly exposed as isolated nunataks close to the coast. Most outcrops of eastern Marie Byrd Land are either situated along Hobbs Coast or form part of the Kohler Range (Fig. 2). Between Demas Range (Hobbs Coast; Fig. 3) and Kohler Range, no rocks are exposed along a coastal stretch of nearly 600 km, with the exception of the young Mt. Siple volcano (Fig. 2). Two rock types dominate exposures. (i) Cenozoic volcanic rocks range in age from ca. 25 Ma to the present. While older volcanic rocks are mostly of basic composition, younger volcanic sequences also comprise more felsic lithologies such as rhyolite and trachyte (LeMasurier and Rex, 1989). (ii) Closer to the coast, most nunataks are composed of granitoid rocks. These range in age from Late Paleozoic (mostly exposed in the Kohler Range) to Late Mesozoic, but are mostly of Cretaceous age (Fig. 2, Table A1). Until ~100 Ma, granitoids are calc-alkaline in character, giving evidence for long-lasting convergence along the Pacific margin of Gondwana. After ~100 Ma, pluton compositions shifted to rift-related alkalic types (i.e., A-type granitoids dominated by syenite, monzonite and monzogranite), marking a change from compressional to extensional tectonic regimes in Marie Byrd Land (Mukasa and Dalziel, 2000).

Mid-crustal melting is inferred to have occurred during the Early Cretaceous (Siddoway et al., 2004), leading to the formation of migmatites, which are today exposed in the Demas Range (Mt. Goorighian and Mt. Prince; Fig. 2), and most spectacularly in the Fosdick Mountains, some 400 km west of this locality. The Demas Range migmatite complex comprises garnet-bearing granite, leucocratic granite, and pegmatite (Mukasa and Dalziel, 2000). Its formation was probably analogously to migmatisation of the Fosdick metamorphic complex in western Marie Byrd Land (Mukasa and Dalziel, 2000). Older (>Cretaceous) high-grade metamorphic basement rocks are rarely exposed. The largest outcrop is

situated at the base of Mt. Murphy volcanic edifice (Kay Peak), containing paragneiss and orthogneiss of Paleozoic age (Pankhurst et al., 1998; Mukasa and Dalziel, 2000). Low-grade metasediments are widely exposed in western Marie Byrd Land (Swanson Formation, Bradshaw et al., 1983), but are nearly absent in eastern Marie Byrd Land. Brand (1979) is the only investigation to have described what are small exposures of low-grade meta-graywacke, arkose, and tremolite-schist (Fig. 2, Table A1). Pankhurst et al. (1998) speculated that the low-grade meta-sediments of the Swanson Formation, or correlatives, extend into eastern Marie Byrd Land beneath the ice. No un-metamorphosed sedimentary rocks are exposed in Marie Byrd Land.

2.3 Climate Evolution of West Antarctica

The climatic evolution of Antarctica is mostly inferred from its surrounding oceanic record. While the long-term evolution of the East Antarctic Ice Sheet is comparably better understood, less data are available for the West Antarctic Ice Sheet and those that are, derive from the Ross Sea due to the lack of drill holes in the Amundsen and Bellingshausen Seas. The first continental ice sheet on Antarctica was formed during Oi-1 cooling at ~34 Ma (Eocene-Oligocene boundary; Miller et al., 1991; Zachos et al., 1992). Whether this only applies to the East Antarctic ice sheet or to one over West Antarctica as well is still debated. From sedimentary evidence, an ice sheet over the Antarctic Peninsula, as part of West Antarctica, has been inferred from the earliest Oligocene (Birkenmajer et al., 2005; Ivany et al., 2006). However, during the Mi-1 glaciation at the Oligocene-Miocene boundary, small ice sheets are considered to have expanded to form one or more continental-scale ice sheets (Zachos et al., 2001). Antarctic ice sheets expanded further during the Middle to Late Miocene and according to Barker and Camerlenghi (2002) the West Antarctic Ice Sheet probably formed at this time. On the basis of geomorphological evidence, Rocchi et al. (2006) argue that since ~15 Ma, Marie Byrd Land has been dominated by cold-based glaciation. During the Pliocene, the West Antarctic Ice Sheet seems to have undergone several collapses (Naish et al., 2009; Pollard and DeConto, 2009). Today, the large glacial systems draining into the Amundsen Sea, namely Pine Island Glacier, Thwaites Glacier, and Smith-Pope-Kohler Glacier, are rapidly thinning and retreating (Rignot et al., 2008 & 2014; Pritchard et al., 2009). There has been about one order of magnitude acceleration in thinning and retreat during the last

few decades as compared with averaged thinning rates since the Last Glacial Maximum (Johnson et al., 2008; Hillenbrand et al., 2013; Larter et al., 2014; Lindow et al., 2014).

3 Methods and material

3.1 Petrographic analysis of ice-transported clasts

Three box cores were retrieved from the western Wrigley Gulf (WG), offshore Hobbs Coast (Fig. 1 & 4). Two of them (PS75/130-2 & PS75/132-1) were taken close to the main glacial outlet of Berry Glacier, PS75/130-2 from top of the last glacial grounding zone wedge (Klages et al., 2014), and PS75/132-1 ocean wards of the grounding zone wedge (Figs. 2; 3b; 4). The third (PS75/133-1) was taken from slightly shallower water depths away from the main glacial trough. The fractions >2 mm were sieved and washed, yielding between ~3 and ~8 kg of clasts per box core. From these samples, a total of 4300 clasts were petrographically described and classified, using microscopic and macroscopic analysis. Additionally, thin section microscopy was used for selected samples.

3.2 Fission track and (U-Th-Sm)/He thermochronology

Fission track thermochronology is based on lattice damages caused by the spontaneous fission of ^{238}U. For apatite, fission track thermochronology is mostly sensitive to temperatures between ~120 and 60°C (=partial annealing zone; Wagner, 1972; Wagner et al., 1989), but is also able to monitor thermal histories involving temperatures below the nominal partial annealing zone (Spiegel et al., 2007). From the detrital samples from the Wrigley Gulf, single-grain age groups are derived using the binomial peak fitting method (Brandon, 1992). For two samples, we also applied zircon fission track (ZFT) thermochronology. This dating method is most sensitive to temperatures between 330 and 230°C (= zircon fission track partial annealing zone; Tagami and Shimada, 1996). No fission track lengths were measured for the zircons.

Apatite (U-Th-Sm)/He (AHe) thermochronology is based on the accumulation of radiogenic ^{4}He in apatite, derived from the radioactive decay of ^{238}U, ^{235}U, ^{232}Th, and ^{147}Sm (Zeitler et al., 1987, Lippolt

et al., 1994). AHe ages, calculated from the ratio between ^{4}He and ^{238}U, ^{235}U, ^{232}Th and ^{147}Sm, reflect the thermal history of a host rock for the temperature range between ~85 and 40°C (= partial retention zone, Wolf et al., 1998). Laboratory details of ZFT, AFT and AHe analysis are provided in the appendix.

Because AFT and AHe dates reflect the length of the pathway travelled by a rock parcel from the depth of the closure isotherm to the surface, AFT and AHe dates depend on sample elevation. Accordingly (i) younger tectonic events are monitored by samples from low elevations, whereas older events are rather stored in high-elevation samples, and (ii), in undisturbed crustal sections, AFT and AHe dates are expected to increase with elevation, with the slope of the age-elevation relationship giving a rough measure for the exhumation rate (Fitzgerald and Gleadow, 1988).

Since the thermal sensitivities of AFT and AHe methods overlap, their results provide independent control for each other. Thus, thermal histories derived from a combination of AFT and AHe dates can be better constrained than thermal histories based on single or non-overlapping thermochronometers. For integrating AFT and AHe ages (and for two samples with ZFT ages as well), we applied thermal history inversions, based on the Ketcham et al. (2007) annealing model, the stopping distances from Ketcham et al. (2011), and the diffusion model of Farley (2000), and using HeFTy software, version 1.8.3. (Ketcham, 2005). Once thermal histories are obtained from inversions, they are interpreted in terms of geodynamic movements of the upper crust. Some basic assumptions underlie these interpretations. (i) Temperature sensitivity of the combined AFT-AHe system can be transferred into crustal depths of 1.3 to 4 km, based on a constant geothermal gradient of 30°C/km during the geological past. However, in a setting with active rifting and magmatic activity such as in West Antarctica, a constant geothermal gradient is unlikely. Therefore, throughout this paper, we use a range of geothermal gradients (70° to 30° C/km) when temperatures are transferred into crustal depths. (ii) Cooling is dynamically interpreted in terms of exhumation; that is, as a rock particle approaches the surface it crosses isotherms. Cooling can also occur, however, in a static fashion through the relaxation of isotherms following emplacement of magmatic bodies. Also, surface uplift (and thus rock uplift) without associated denudation will not result in cooling and is thus not detected by

thermochronological methods. (iii) Because cooling is associated with denudation, cooling rates can be transferred into denudation rates (again under the assumption of a certain geothermal gradient value). These denudation rates are often interpreted as erosion rates. In West Antarctica, however, tectonic denudation certainly plays a major role, which is why we mostly use the more neutral term "denudation" instead of "erosion" throughout this paper. (iv) Thermochronology does not give direct evidence for topographic evolution, but can nevertheless be used as a proxy in that a low relief area with subdued topography will normally be related to lower (erosional) denudation rates than high standing topography with strong relief. However, in a setting such as West Antarctica, extension and normal faulting may have resulted in low topography concurrent with rapid footwall exhumation and thus high (tectonic) denudation rates.

3.3 Sampling strategy

For thermochronology sampling, we targeted outcrops of granitoid and gneiss from the Mount Murphy area, Kohler Range and Hobbs Coast (Figs. 2 & 3, Table A2). For the Mount Murphy area, we collected samples from basement rocks exposed at the north-eastern margin of Mt. Murphy (Kay Peak) and from a gabbroic intrusive body about 25 km south of Mt. Murphy (Dorrel Rock; Fig. 3). For the Kohler Range and Hobbs Coast areas, mostly granitoid rocks from coastal nunataks were sampled (Figs. 2 & 3, Table A2). All samples are situated at the margins of the Marie Byrd Land Dome (Fig. 1). Cenozoic volcanic rocks were not collected, because they usually do not contain sufficiently large apatite crystals and because they do not contain information about denudation. Sampling for this study mostly took place in 2010 during cruise ANT XXVI/3 of research vessel *Polarstern* (Gohl, 2010), using helicopter support for onshore sampling (MBL sample codes, Table A2). The 2010 sample set was complemented by samples from the 1990-1993 SPRITE campaign (DiVenere et al., 1993; MB sample codes; Table A2), which was the last major land expedition to explore Marie Byrd Land.

Since thermochronology data can be sensitive to relative sample elevation, sampling campaigns for AFT and AHe dating usually involve the collection of samples from vertical and horizontal profiles. Due to the limited time available in the field and, more importantly, outcrop constraints in Marie Byrd Land, vertical sampling could not be undertaken. The main problem with the distributed sample set

being limited to nunataks (areas of high elevation) is that it excludes low-elevation samples (beneath the ice all over Marie Byrd Land) that potentially monitor the younger part of the tectonic history of the region. To address this problem, we took box cores from the marine realm (Wrigley Gulf offshore Hobbs Coast, close to the main outlet of Berry Glacier; Figs. 1 & 3; Table A2; PS sample codes). The clastic sediments retrieved from the box cores are derived from the continental hinterland and were eroded and transported to the marine realm by glacial activity. Thus, apatite grains obtained from these sediments monitor the denudation history integrated over the whole glacial catchment including higher elevated areas as well as the areas beneath the deeply incised glacial valleys. Furthermore, the clasts and lithic fragments also provide petrographic information on the sub-ice lithology of the source area.

4 Results and interpretation

4.1 Petrographic description of clasts from Wrigley Gulf – implications for sub-ice lithology in Marie Byrd Land

The two box cores taken close to the main glacial trough of Berry Glacier show largely similar lithologies, whereas the box core from the more distal position slightly differs in the composition of its clasts (Fig. 4). Not surprisingly, the dominant lithologies in all three box cores are igneous rocks, either of granitic to dioritic compositions and obviously derived from the Paleozoic to Cretaceous batholiths developed along the paleo-Pacific margin of Gondwana, or of volcanic rocks derived from Cenozoic volcanism throughout Marie Byrd Land. The latter group consists of basalt, rhyolite (only in box core PS75/133-1; Fig.A1), hyaloclastite, and few felsic rocks. Even some volcanic rocks with high erodibility, such as tuff, have survived glacial transport to reach the marine sink relatively intact (Fig. 4).

One large Qtz-Monzonite pebble is cut by pseudotachylite veins (Fig. A1-A). Viewed in thin section, most minerals of this rock show brittle deformation, and only quartz shows fine-grained recrystallisation along cracks and crystal margins. This indicates that part of the glacial catchment area experienced tectonic deformation at the brittle-ductile transition.

Conspicuous are slightly deformed, light-coloured granite clasts containing small euhedral garnets (Fig. A1-C). These are very similar to rocks described from exposures of Mt. Goorighian / Demas migmatite complex (Mukasa and Dalziel, 2000). Furthermore, two box cores contain basic granulite, i.e., coarse, granular basic rocks with large garnets (Fig. A1-D), showing that high-grade rocks are more abundant in eastern Marie Byrd Land than suggested by the lithologies of the exposed nunataks. Both, the garnet-granites and the basic granulites probably represent equivalents of the Fosdick metamorphic complex of western Marie Byrd Land (Siddoway et al., 2004; Korhonen et al., 2010). Also interesting is the occurrence of fine-grained greenschist-facies metamorphic rocks in two of the box cores (Figs. A1-E &-F), which may indicate that the Swanson Formation of western Marie Byrd Land extends farther to the east of known outcrops and beneath glacial cover, as earlier proposed by Pankhurst et al. (1998). The low-grade metamorphic rocks in the box core consist of quartz, feldspar, sericite and chlorite. Thin section analysis shows that part of the samples also contain epidote, clinozoisite, and tremolite, indicating that some of the low-grade rocks are not of sedimentary origin but may rather be derived from basaltic rocks. Similar compositions were reported from small exposures of the western Hobbs Coast (Brand, 1979), but, to the knowledge of the authors, not from Swanson Formation of western Marie Byrd Land. However, whether or not Swanson Formation or correlative facies extend into this area, our data strongly indicate that the host rocks into which the coastal batholiths intruded, were composed of low-grade greenschist-facies metamorphic rocks.

To a very minor amount, all box cores comprise semi-lithified fine-grained rocks of seemingly sedimentary origin, containing larger rock fragments (Figs. A1-G & -H). Although we have classified these as "tillite", we cannot exclude a volcanic origin, or in-situ formation in the marine sink. In any case, sedimentary rocks make up only a very small proportion of the clasts, in line with the composition of exposed nunataks, where sedimentary rocks are absent. However, the lack of sedimentary clasts in the box cores is no real evidence for the absence of sedimentary rocks in the source area, as they may simply have not survived the glacial transport. On the other hand, other "weak" lithologies such as hyaloclastite, slates, and tuff did evidently survive glacial transport mechanisms, hence large sub-ice occurrences of sedimentary rocks in eastern Marie Byrd Land seem unlikely.

321 *4.2 AFT analysis of clasts from Wrigley Gulf*

322 Two box core samples were analysed by AFT thermochronology; one sample (PS75/130-2) from
323 relatively close to the axis of the glacial trough and the other more from its margin (PS75/133-1; Fig.
324 4). Each sample yielded two age groups: one of 74 ± 4 Ma and 79 ± 6 Ma, and another of 20 ± 7 Ma
325 and 61 ± 10 Ma (Fig. 5; Table 1). The older age groups in both samples overlap within errors and
326 overlap with AFT ages for exposures from onshore Hobbs Coast (see next section). Accordingly, they
327 are interpreted as being derived from basement rocks with similar cooling histories as those from the
328 nunatak exposures, showing that large parts of the catchment area experienced a thermal history
329 dominated by Cretaceous cooling. The younger age group of sample PS75/133-1 (61 ± 10 Ma) also
330 seems to mostly reflect (Late) Cretaceous-Paleocene cooling and is interpreted as being derived from
331 the same basements rock succession as those exposed along Hobbs Coast but from lower structural
332 levels, and/or from slightly later exhumation. Of particular interest is the 20-Ma age group of sample
333 PS75/130-2 as no basement rocks with similar ages are known from Hobbs Coast exposures. However,
334 some of the Marie Byrd Land dome volcanoes have similar ages, namely Mount Petras and Mount
335 Flint of the McCuddin Mountains (Fig. 2, LeMasurier, 2006). These volcanoes are however exposed
336 south of the catchment area of Berry glacier. It is of course possible that other volcanoes of similar age
337 are hidden beneath ice of the Berry glacial catchment. We nevertheless consider a volcanic source for
338 the 20-Ma age group unlikely, because (i) according to the volcanic age pattern described by
339 LeMasurier (2006), volcanoes of the Marie Byrd Land dome become increasingly younger towards the
340 coast (i.e., towards the catchment area of Berry glacier); (ii) the lithologies of Marie Byrd Land
341 volcanoes (mostly basalt and rhyolite) are unlikely to contain apatite; and (iii) the volcanic lithologies
342 that may contain apatite (mostly tuff) usually yield euhedral pristine crystals, and these were not
343 observed in the apatite grains contained in the 20 Ma-age group. We thus interpret the 20-Ma age
344 group as being derived from basement rocks deeply incised beneath the Berry glacier valley, in line
345 with the position of the box core close to the axis of the glacial trough. If this is the case, then the 20-
346 Ma age group reflects Miocene or post-Miocene cooling of basement in the source area.

347 *4.3 Thermochronology data for Hobbs Coast and Kohler Range*

AFT data from the Hobbs Coast and the Kohler Range are very similar, yielding mostly late Cretaceous ages around 70 Ma, with only two older ages of ~90 Ma, both from the Kohler Range (Fig. 3; Table 2). Mean track length and Dpar values are also similar, with track lengths ranging between 14.5 µm and 13 µm, and Dpar values clustering around 2 µm. All samples pass the Chi^2-test at the 5% level, indicating that the samples are kinetically homogeneous. For both areas, no clear age-elevation relationships are observed, indicating that the sampled nunataks are separated by faults (Fig. A2). This observation is in line with previous field observations (LeMasurier and Landis, 1996).

Three aliquots were excluded from the AHe data set, since they are obviously too old, which we explain by He-producing micro-inclusions such as zircon or monazite, too small to be detected by microscopy (Table 3). Two aliquots from the Mt. Goorhigian (Hobbs Coast) yielded non-replicating dates; and the sample did not contain sufficient apatite for AFT analysis. Therefore, the data for this sample are shown in Fig. 3 and Table 3, and have not been further interpreted. Along the same lines, apatite yield and grain quality for sample MBL-57-10 from Kohler Range only allowed one aliquot to be dated. This is shown in Fig. 3 and Table 3, but it is not included in thermal history modelling. The remaining aliquots yielded Late Cretaceous to Eocene AHe ages. Age patterns in the Hobbs Coast and Kohler Range samples are similar. As for the AFT data, no clear age elevation relationship is observed, and in the Kohler Range area is seems that there may be an inverted relationship, with youngest AHe ages being associated with the highest sample elevations (Fig. A2).

For thermal history inversions we focused on samples having both AFT and AHe data. The resulting thermal histories show similar patterns for all sample data (Fig. 6). One sample, MB-163-1M from Mt. Goorhigian (Hobbs Coast) only yielded statistically acceptable fits. As this solution is based on two thermochronometers with overlapping thermal sensitivities, we still consider the resulting time-temperature history as reliable. Of particular interest is sample MBL-51-10 from Kohler Range (Fig. 3a). Despite 100 000 paths in Monte Carlo simulations, very few statistically good solutions emerged for this sample. Thus, variation of statistical possible solutions is small and the thermal history of this sample is therefore tightly constrained, whereas the thermal histories of the other samples cover a broader range of statistically possible solutions. Thermal histories derived for all samples from Kohler

Range and Hobbs Coast are characterized by relatively rapid cooling (as compared to the later cooling periods) during the mid to Late Cretaceous (~5-13°C/Ma), followed by slow cooling through to the early Miocene (<1°C/Ma), which was followed by renewed more rapid cooling (2-3°C/Ma) to present-day ambient temperatures. Only the thermal history for the sample from Wunneburger Rock north of Kohler Range differs from this pattern in having the rapid Cretaceous cooling episode start earlier (at ~100 Ma), and in having the Miocene cooling episode starting later (after approximately10 Ma). Its thermal history is thus similar to samples from the Pine Island Bay/Thurston Island block (Lindow, 2014).

4.4 Thermochronology data for the Mount Murphy area

AFT ages from the Mt. Murphy area cluster tightly between 28 and 31 Ma, with MTLs between 13.1 and 14.5 µm and Dpar values of ~1.9 µm (Fig. 3; Table 2, samples MBL-60-10, MBL-61-10, MBL-63-10). The age-elevation relationships for these samples are also inverted, with the youngest AFT ages being associated with the highest elevations (Fig. A2). The same also applies to the AHe ages. These cluster between 25 and 18 Ma (Figs. 3 and A2; Table 3). The youngest age is for the gabbro sample from Dorrel Rock (MBL-61-10) and is based on only one single-grain aliquot. We also analysed two more aliquots for this sample consisting of very large apatite grains, but with very irregular morphologies, which rendered them impossible to make alpha ejection corrections. To avoid the need for this correction, we mechanically abraded the outer ~30 µm of two grains (Spiegel et al., 2009). The resulting ages are 34 and 38 Ma, significantly older than all other AHe ages from the Mt. Murphy area, and more importantly, older than the corresponding AFT age, and even older than the crystallization age of Dorrel Rock gabbro as reported by Rocchi et al. (2006). Thus, these two grains either contained micro-inclusions or the "too-old" dates are the result of abrasion. Abrasion leads to the selected measurement of only the central part of the diffusion profile, which, for samples with diffusion-controlled profiles, may cause over-estimation of AHe ages (Farley, 2002). In any case, both aliquots were excluded from further interpretation. Thermal history inversion yields similar cooling patterns for all three samples, with rapid cooling during the Oligocene (~5°C/Ma), slowing slightly during the early Miocene (~3°C/Ma; Figs. 6 & 7).

Although Mt. Murphy volcano was active only at 8 Ma, the surrounding area had already experienced intrusive magmatic activity during the Early Oligocene (Dorrel Rock gabbro, Rocchi et al., 2006). Thus, it could be argued that the thermochronology data obtained from this area cannot be interpreted in terms of exhumation; rather, it may reflect isotherm relaxation following heating associated with magmatic activity. We argue against this "static" interpretation because (i) the rapid cooling to near-surface temperatures following the time of magmatic intrusion does not fit a scenario of isotherm relaxation; (ii) other isotopic systems previously applied to the exposures at Kay Peak do not show disturbances by Oligocene magmatic activity, having yielded Paleozoic ages for orthogneisses and a Permian age for the granite (Pankhurst et al., 1998; Mukasa and Dalziel, 2000); (iii) Dorrel Rock gabbro, currently exposed at ~700 meters above sea level (m.a.s.l)., was intruded during the Early Oligocene at a crustal depth of at least 3 km (Rocchi et al., 2006). Therefore, the host rock for this sample must have experienced relatively rapid Oligocene and post-Oligocene erosion, in line with a dynamic interpretation of cooling history; and finally (iv), the cooling history derived from the thermochronology data is in astonishingly good agreement with the erosion history previously suggested by Rocchi et al. (2006) on the basis of independent evidence, giving further confidence to interpreting the thermochronology data in terms of dynamic exhumation.

5 Discussion

5.1 Structural evolution of Marie Byrd Land – implications for Cenozoic rifting along Pine Island Bay

Figure 7 shows the weighted mean thermal histories for all samples analysed for AFT and AHe data. The host rocks from Hobbs Coast and Kohler Range show largely similar cooling patterns, whereas the thermal history of Wunneburger Rock north of the Kohler Range differs and in contrast shows similarities with the cooling patterns for host rocks in the Pine Island Bay area (Lindow, 2014). Thus we conclude that a fault with significant displacement separates Wunneburger Rock from Kohler Range. Assuming that there is topographic expression of the fault structure, we have mapped the fault along a valley between Wunneburger Rock and Kohler Range (thin dotted blue line, Fig. 8). This

valley runs parallel to the coast and parallel to tectonic structures resulting from Late Cretaceous West Antartica-Zealandia separation (Gohl, 2012; Gohl et al., 2013a). Thus we interpret the fault as being related to Late Cretaceous continental extension and breakup.

Most striking are the strongly contrasting cooling histories between Hobbs Coast and Kohler Range on one side and the Mt. Murphy area on the other (Figs. 6 & 7). This implies that a major tectonic boundary separates these areas. Furthermore, thermochronology data for eastern Pine Island Bay (Thurston Island block east of the Mt. Murphy area) show a different thermal evolution, with rapid cooling throughout the mid and Late Cretaceous, followed by very slow cooling during the entire Cenozoic (Lindow, 2014). Thus, the Mt. Murphy area is characterised by rapid Cenozoic exhumation compared with surrounding areas that displayed slow exhumation.

A logical explanation for rapid exhumation during the Oligocene would be enhanced erosion due to the onset of continental glaciation (e.g., Wilson et al., 2013). However, the isolated character of the Mt. Murphy erosion history rules climate out as a steering factor for exhumation. Instead, we explain exhumation of the Mt. Murphy block as a horst that was tectonically exhumed during rifting along adjacent Pine Island Bay. This interpretation underscores previous suggestions that Pine Island Bay may form a rift branch connecting the WARS with Amundsen Sea (Jordan et al., 2010; Gohl et al., 2013a,b); and it also puts rifting into a temporal framework, thereby providing the first direct evidence for Cenozoic rifting outside the Ross Sea area. Note, however, that our proposed Mt. Murphy Rift is located along the western margin of Pine Island Bay, whereas previous suggestions have placed rift branches reaching Amundsen Sea along the paleo-trough of Pine Island Glacier; that is, along the eastern part of Pine Island Bay (Fig. 8).

Our interpretation of the Mt. Murphy area as being influenced by rift tectonics is based on the following arguments and observations: (i) thermochronology data clearly reveal differential exhumation histories for the Thurston Island block (Lindow, 2014), the Mt. Murphy area, and the Kohler Range / Hobbs Coast, requiring tectonic boundaries in between that were active during and possibly after the Oligocene; (ii) thermochronology data shows that the eastern side of Pine Island Bay was tilted towards the Pine Island Trough post-Cretaceous, corroborating Cenozoic tectonic activity

along Pine Island Bay (Lindow, 2014); (iii) Oligocene igneous activity as described for the Mt. Murphy block (Dorrel Rock gabbro, Rocchi et al., 2006) is unique in Marie Byrd Land because no other Cenozoic intrusive bodies are described, because it is significantly older than the volcanic activity of the Marie Byrd Land dome, which commenced at ~29 to 25 Ma (LeMasurier, 2006), and because it is at odds with the magmatic age patterns of the Marie Byrd Land dome, showing the oldest magmatic activity in the centre of the dome and the youngest at its margins (LeMasurier and Rex, 1989). Thus we suggest that Dorrel Rock gabbro intruded in response to Cenozoic rifting along Pine Island Bay, exploiting the active boundary fault of the rift situated along the Mt. Murphy block (Mt. Murphy Rift; Fig. 8). In that respect, it is interesting to note that the present-day heat flow along this supposed boundary fault still seems to be strongly elevated (Schroeder et al., 2014 – note, however, that their data do not fully reach the Mt. Murphy area); (iv) the only other area of Antarctica also showing Oligocene exhumation is also associated with rifting along the WARS - the Transantarctic Mountains. Exhumation of the Transantarctic Mountains has been traditionally described as episodic, with two major exhumation pulses starting during the Late Cretaceous and the Eocene (Balestrieri et al., 1994, 1997; Fitzgerald, 2002; Lisker, 2002). Modelling of these older data taking into account new independent geological evidence recently led to re-interpretation of the exhumation history: at least the northern Transantarctic Mountains experienced uniform exhumation, starting at the Eocene-Oligocene boundary (Prenzel et al., 2013, 2014). Thus, rift shoulder uplift along the "big rift" would be contemporaneous with its "little brother", the Mt. Murphy rift shoulder adjacent to Pine Island Bay.

In Fig. 8, we tentatively show structural elements of the WARS as implied by interpretation of the thermochronology data reported here. Based on our data, we place the rift branch close to the Mt. Murphy area, extending northwards into the Amundsen Sea Embayment and southwards into a morphological depression that cuts the Byrd Subglacial Basin. If our model is valid, and if the Mt. Murphy Rift was active contemporaneously with the Ferrigno Rift in the Bellingshausen Sea sector (Bingham et al., 2012), then both branches would be characterized by transtension. This is in agreement with the suggestion of Müller et al. (2007) who proposed early Cenozoic dextral transtension along a rift branch reaching into Bellingshausen Sea. Dextral transtension along the Ferrigno Rift, coeval with sinistral transtension along the Mt. Murphy Rift, would lead to north-

eastward movement of the Thurston Island Block, thus causing the crustal extension along the Pine Island Rift (Jordan et al., 2010) and also along the Byrd Subglacial Basin (Fig. 8). This model kinematically links previously described areas of crustal extension, i.e., the Ferrigno Rift reaching into Bellingshausen Sea, Pine Island Rift beneath the main trunk of Pine Island Glacier, and the deeply incised Bentley Subglacial Trench and Byrd Subglacial Basin in the interior of the rift. It also explains the geometric relationship amongst these structures; that is, the odd angles between Ferrigno Rift and Pine Island Rift and between Bentley Subglacial Trench and Byrd Subglacial Basin.

The fault separating the Mt. Murphy block from Kohler Range was placed along a valley running parallel to Mt. Murphy Rift and Pine Island Bay, and also parallel to faults directly adjacent to the Mt. Murphy volcanic edifice described by LeMasurier (1972). Accordingly, we interpret the ridges and valleys parallel to Pine Island Bay as morphological expressions of horst-and-graben-systems derived from block faulting caused by extension along Mt. Murphy Rift. However, due to extensive glacial cover, the exact locations of faults remain speculative, including other possible fault locations, such as one following the Smith Glacier trough.

5.2 Denudation history of Marie Byrd Land – implications for topographic evolution and onset of continental glaciation

Since ~100 Ma, Marie Byrd Land has been affected by crustal extension (Mukasa and Dalziel, 2000) and after~90 Ma an erosion surface evolved, bevelling the coastal batholiths of West Antarctica. This implies a Late Cretaceous, rather low-lying topography across Marie Byrd Land, close to sea level. Between 90 and 60 Ma, the basement beneath eastern Marie Byrd Land (this study), western Marie Byrd Land (Richard et al., 1994; Adams et al., 1995; Lisker and Olesch, 1998) and the Pine Island Bay area (Lindow, 2014) experienced rapid cooling (Figs 6 & 7). Because of the extensional setting and the low-lying topography, we explain rapid cooling (with rates up to 30 to 40°C/Ma; Lindow, 2014) as resulting predominantly from tectonic denudation rather than from erosional denudation.

All samples from Hobbs Coast, Kohler Range and Pine Island Bay area largely follow similar cooling patterns, although the timing of Late Cretaceous cooling – even of neighbouring samples – varies between 90 and 60 Ma, with no apparent pattern (Fig. 7). We explain this variation as a result of extensional tectonics, leading to horst-and-graben formation juxtaposing rocks from different crustal levels. Block faulting also explains the partly inverted age elevation relations, with young ages associated with high elevations and old ages associated with low elevations.

At ~60 Ma, rapid cooling ceased, indicating that the first rifting episode of the WARS lasted until that time. The second rifting episode, also indicated by rapid cooling and only recorded by the rocks of the Mt. Murphy area, lasted from Early Oligocene until Early Miocene or later (Fig 7). For all investigated rocks except for those from the Mt. Murphy area (where Cretaceous and Early Cenozoic cooling is not recorded), rapid cooling during the first rifting episode was followed by very slow cooling that lasted until ~20 Ma (and longer than that for the Wunneburger Rock site; Fig. 7). We interpret this slow cooling period as slow erosional downwearing related to formation of the West Antarctic erosion surface. If this is valid, it implies that formation of the erosion surface across Marie Bryd Land outlasted by ~55 Ma that across Campbell Plateau and parts of New Zealand side.

Also by ~60 Ma, all samples (with the exception of the Mt. Murphy samples) have cooled to temperatures below ~60°C, indicating low denudation rates and net denudation of less than 1 to 2 km (assuming a range of geothermal gradients from 30°C to 70°C/km). Similar data are obtained for Cenozoic net denudation in western Marie Byrd Land (Richard et al., 1994; Adams et al., 1995; Lisker and Olesch, 1998), the Pine Island Bay area (Lindow, 2014), and the Ellsworth Mountains (Fitzgerald and Stump, 1992). Such low denudation rates fit with a scenario of tectonic quiescence and lack of significant relief, in agreement with ongoing formation of the West Antarctic erosion surface close to sea level. In particular, no erosional response (within the sensitivity limits of low-temperature thermochronology) to assumed onset of continental glaciation at the Eocene-Oligocene boundary is observed. This is in contradiction to offshore seismic data which indicate large volumes of glacially-derived sediment deposited along the West Antarctic margin and continental shelf above the Eocene-Oligocene boundary (Wilson et al., 2012). On the other hand, in the absence of drill core data, both

provenance and stratigraphy of the offshore deposits are poorly constrained. We suggest that at least part of post-Eocene strata deposited offshore West Antarctica was derived from the Transantarctic Mountains. These experienced rapid erosion at around the Eocene-Oligocene boundary (Prenzel et al., 2013, 2014), and since the Neogene, between 3 and 5 km of overburden was removed from that area (Zattin et al., 2014). Also, unlike West Antarctica, glaciation of the Transantarctic Mountains already at the Eocene-Oligocene boundary is relatively well-constrained (Barker et al., 2007).

As emphasized by Barker et al. (2007), the uplift history of the Marie Byrd Land dome is an important uncertainty that needs to be addressed for better constraining West Antarctic glaciation history. Our thermochronology data from the flanks of the Marie Byrd Land dome do not give evidence for enhanced denudation at the Eocene-Oligocene boundary, but rather suggest accelerated denudation since ~20 Ma, i.e. the early Miocene. These data provide the first direct evidence on the timing of Marie Byrd Land dome denudation, however, it should be kept in mind that the Miocene denudation history presented in this study is chiefly based on two samples:

(i) Thermal history modelling of sample MBL-51-10 from the Kohler Range yields tightly constrained time-temperature paths, dating the onset of accelerated cooling at ~20 Ma. The other samples from the Marie Byrd Land dome are in agreement with this cooling history, but are less tightly constrained and also allow for other solutions. Furthermore, the samples from the Hobbs Coast area have already cooled to temperatures below the apatite partial annealing and partial retention zones at 20 Ma and are thus outside the temperature range where the applied thermochronometers are most sensitive (although Spiegel et al. (2007) showed that apatite fission track analysis is able to monitor thermal histories within temperature ranges well below the nominal partial annealing zone). In any case, net denudation of onshore exposures since the early Miocene was associated with cooling of only ~35 to 50°C for the nunataks of the Kohler Range and Hobbs Coast area. Net cooling can be translated into net denudation ranging between 1.2 to 1.7 km (assuming a geothermal gradient of 30°C/km) and 0.5 to 0.7 km (assuming a geothermal gradient of 70°C). This underscores earlier observations made by Rocchi et al. (2006) that uplift of the Marie Byrd Land dome outpaced erosion.

561 (ii) The second sample suggesting enhanced early Miocene denudation is sample PS 75/130-2. It
562 contains an early Miocene age group, indicating that at least small subglacial areas within the
563 catchment of Berry Glacier experienced sufficient cooling and denudation to expose 20-Ma AFT ages,
564 that is, net cooling of at least 120°C and thus net denudation of >1.7 to 4 km since the Early Miocene.
565 This agrees with improved bedrock topography of the Marie Byrd Land dome area as presented by
566 Holschuh et al. (2014). Their data show a deeply incised trough in the hinterland of the Getz Ice Shelf
567 (Fig. 3b) and close to the Berry Glacier, reaching up to 1000 m below sea level and extending over
568 200 km towards the continental interior. Thus, based on these two samples, we tentatively suggest that
569 denudation of the Marie Byrd Land dome started at ~20 Ma, implying that uplift and thus relief
570 formation also only started at 20 Ma, nearly 10 m.y. later than previously suggested. Of course it is
571 possible that uplift started earlier and was simply not associated with denudation. On the other hand, if
572 at 20 Ma, uplift and relief formation was associated with the start of (erosional) denudation, then why
573 should the erosional response be different for uplift and relief formed at ~30 Ma? In any case, if our
574 assumption that the Marie Byrd Land dome only started uplifting during the Early Miocene is valid,
575 this would imply the following:

576 (i) Current paleo-topographic models assuming elevations of the Marie Byrd Land dome of up to
577 ~1000 m at the Eocene-Oligocene boundary as the maximum end of the estimated topographic range
578 by Wilson et al. 2012) would likely overestimate the early topographic evolution of this region; and (ii)
579 large-scale continental glaciation over coastal West Antarctica, requiring significant areas of emerged
580 land, may have only occurred since the Early Miocene. This second implication is again in contrast to
581 the large volume of glacially derived sediments on the continental shelves and rise of the Pacific realm
582 of West Antarctica used by Wilson et al. (2012) to calculate the volumes of eroded sediment, at least,
583 if these sediments are indeed derived from West Antarctica. For better constraining the erosion history
584 of the Marie Byrd Land dome and thus boundary conditions for West Antarctic glaciation, more
585 research is required, particularly involving (i) more thermochronology data, focusing on detrital
586 samples from the Getz area, (ii) sediment drilling in the Amundsen Sea, providing stratigraphic and
587 provenance information for offshore seismic data, and (iii) sediment budget calculations reconciling

588 erosion rates from the Transantarctic Mountains and onshore West Antarctica based on
589 thermochronology data with volumes of marine strata calculated from offshore seismic studies.

590

591 **6 Conclusions**

592 For this study, we used apatite fission track and (U-Th-Sm)/He thermochronology data as well as the
593 results of petrographic analysis of marine sedimentary clasts to decipher the tectonomorphic evolution
594 of Marie Byrd Land and to characterize subglacially exposed lithologies. The following conclusions
595 can be drawn from our data:

596 (1) Petrographic analyses showed that host rocks for the coastal batholiths of Marie Byrd Land
597 were most likely low-grade meta-sediments, presumably equivalent to the early Paleozoic
598 Swanson Formation exposed farther west in the Ford Ranges. Also, high-grade rocks likely
599 related to Cretaceous metamorphism and anatexis are subglacially exposed and may be
600 equivalent to the Fosdick migmatite complex in the Ford Ranges. This suggests that the
601 geological setting as described for western Marie Byrd Land continues subglacially into the
602 Hobbs Coast area of eastern Marie Byrd Land.
603 (2) Thermochronological analyses showed that all of coastal Marie Byrd Land experienced
604 relatively rapid denudation during the Late Cretaceous, most likely in response to extensional
605 tectonics. This dates early rifting in the WARS to the period between >100 and 60 Ma.
606 (3) Apatite fission track and (U-Th-Sm)/He ages of the Mt. Murphy area strongly differ from
607 those of surrounding areas, indicating that the Mt. Murphy area constitutes a fault-bound block
608 exhumed since the Early Oligocene. We interpret this exhumation to be a response to
609 Oligocene rifting along Pine Island Bay, probably contemporaneous with the Ferrigno Rift,
610 leading to northeastward movement of the Thurston Island block, and extension beneath the
611 main trunk of Pine Island Glacier and in the Byrd Subglacial Basin.
612 (4) Between Late Cretaceous and Early Miocene, eastern Marie Byrd Land was characterized by
613 very low denudation rates, which we explain as reflecting tectonic quiescence, a subdued

topography, and the formation of the West Antarctic erosion surface close to sea level. According to this scenario, only limited land areas may be emergent for supporting the formation of a continental ice sheet at the Eocene-Oligocene boundary.

(5) Based chiefly on the thermochronology data of two samples, we tentatively date the onset of erosion of the Marie Byrd Land dome at ~20 Ma. Assuming erosion started contemporaneously with uplift, this dome dates from the early Miocene, nearly 10 Ma later than previously suggested. The topographic evolution has likely affected the early glaciation history, ostensibly triggering more intense glaciation from 20 Ma onwards.

Acknowledgements

This study was financially supported by the German Science Foundation DFG, grant no SP 673/6-1, in the framework of the Priority Programme SSP 1158 "Antarctic Research with comparative investigations in Arctic ice areas". We specially thank Captain Uwe Pahl of RV Polarstern and his crew, Klaus Hammrich and Hans Heckmann from Heli Service International, Mirko Scheinert and Ralf Rosenau (TU Dresden) for their support during sampling, Anke Toltz and her team of students assistants (University of Bremen) for sample processing, and Barry Kohn (University of Melbourne) for his support regarding apatite (U-Th-Sm)/He analysis. Two anonymous reviewers are thanked for their insightful comments that helped improve an earlier version of this paper, and Sierd Cloetingh is thanked for the editorial handling.

References

Adams, C.J., Seward, D. and Weaver, S.D., 1995. Geochronology of Cretaceous granites and metasedimentary basement on Edward VII Peninsula, Marie Byrd Land, West Antarctica. Antarctic Science, 7 (3): 265-276

Balestrieri, M.L., Bigazzi, G., Ghezzo, C. and Lombardo, B., 1994. Fission track dating of apatites from the Granite Harbour Intrusive Suite and uplift-denudation history of the Transantarctic Mountains in the area between the Mariner and David Glaciers (northern Victoria Land, Antarctica). Terra Antartica (1): 82–87.

Balestrieri, M.L., Bigazzi, G. and Ghezzo, C., 1997. Uplift-denudation of the Transantarctic Mountains between the David and the Mariner glaciers, northern Victoria Land (Antarctica); constraints by apatite fission-track analysis. In: Ricci, C.A. (Ed.), The Antarctic Region; Geological Evolution and Processes; Proceedings of the VII International Symposium on Antarctic Earth Sciences. Terra Antartica: 547–554.

Barker P.F. and Camerlenghi, A., 2002. Glacial History of the Antarctic Peninsula from Pacific Margin Sediments, Barker, P.F., Camerlenghi, A., Acton, G.D., and Ramsay, A.T.S. (Eds.) Proceedings of the Ocean Drilling Program, Scientific Results Volume 178.

Barker, P., Diekmann, B. and Escutia, C., 2007. Onset of Cenozoic Antarctic glaciation. Deep-Sea Research II 54, 2293-2307.

Bingham, R., Ferraccioli,, F., King, E., Larter, R., Pritchard, H., Smith, A. and Vaughan, D., 2012. Inland thinning of West Antarctic Ice Sheet steered along subglacial rifts. Nature, 487, 468-471.

Birkenmajer, K., Gaździcki, A., Krajewski, K.P., Przybycin, A., Solecki, A., Tatur, A., and Yoon, Ho Il, 2005. First Cenozoic glaciers in West Antarctica. Polish Polar Research, 26 (1): 3–12.

Boulton, G., 2006. Glaciers and their coupling with hydraulic and sedimentary processes, Knight, P. (Ed) Glacier Science and Environmental Change. Blackwell Publishing, 544 pp.

Bradshaw, J.D., Andrew, P.B. and Field, B.D., 1983. Swanson Formation and related rocks of Marie Byrd Land and a comparison with the Robertson Bay Group of northern Victoria Land. *In:* Oliver, R.L., James, P.R. and Jago, J.B. (eds.) Antarctic Earth Science. Cambridge University Press, Cambridge, 274-279.

Brand, J.F., 1979. Low grade metamorphic rocks of the Ruppert and Hobbs Coasts of Marie Byrd Land, Antarctica. M.Sc. Thesis Texas Tech University, 49 pp.

Brandon, M.T., 1992. Decomposition of fission-track grain-age distributions. American Journal of Science, 292: 535–564.

Brandon, M.T., 2002. Decomposition of mixed grain age distributions using Binomfit. On Track, 24: 13–18.

Busetti, M., Spadini, G., Van der Wateren, F. M., Cloetingh, S. and Zanolla C., 1999. Kinematic modelling of the West Antarctic Rift System, Ross Sea, Antarctica. Global and Planetary Change, 23 (1-4): 79 – 103.

Cande, S.C. and Stock, J.M., 2004. Pacific-Antartic-Australia motion and the formation of the Macquarie Plate. Geophysical Journal International, 157: 399-414.

Cande, S.C., Stock, J.M., Müller, R.D. and Ishihara, T., 2000. Cenozoic motion between East and West Antarctica. Nature, 404: 145-150.

Dalziel, I.W.D., 2006. On the extent of the active West Antarctic rift system. Terra Antartica, 12: 193-202.

Dalziel, I.W.D. and Elliot, D.H., 1982. West Antarctica: Problem Child of Gondwanaland. Tectonics, 1(1): 3-19.

DiVenere, V.J., Bradshaw, J.D., Weaver, S.D., Palais, D.G., Pankhurst, R.J. and Storey, B. C., 1993. Geological investigations in eastern Marie Byrd Land, West Antarctica. Antarctic Journal of the United States, 28 (5): 5-6.

DiVenere, V.J., Kent, D.V. and Dalzier, I.W.D., 1994. Mid-Cretaceous paleomagnetic results from Marie Byrd Land, West Antarctica: A test of post-100 Ma relative motion between East and West Antarctica. Journal of Geophysical Research, 99 (B8): 15,115 – 15,139.

Eagles, G., Gohl, K. and Larter, R.D. (2004). High-resolution animated tectonic reconstruction of the South Pacific and West Antarctic margin; Geochemistry, Geophysics, Geosystems 5/7, doi:10.1029/2003GC000657.

Eagles, G., Larter, R.D., Gohl, K. and Vaughan, A.P.M. (2009).West Antarctic Rift System in the Antarctic Peninsula. Geophysical Research Letters 36, L21305, doi:10.1029/2009GL040721.

Farley, K. A., 2000. Helium diffusion from apatite: General behavior as illustrated by Durango fluorapatite. Journal of Geophysical Research, 105, (B2): 2903-2914.

Farley, K.A., 2002. (U–Th)/He dating: techniques, calibrations, and applications. Reviews in Mineralogy and Geochemistry, 47: 819–844.

Fitzgerald, P.G., 2002. Tectonics and landscape evolution of the Antarctic plate since the breakup of Gondwana, with an emphasis on the West Antarctic Rift System and the Transantarctic Mountains. Royal Society of New Zealand Bulletin, 35: 453–469.

Fitzgerald, P.G. and Gleadow, A.J.W., 1988. Fission-track geochronology, tectonics and structure of the Transantarctic Mountains in Northern Victoria Land, Antarctica. Chemical Geology: (Isotope Geoscience Section), 73 (2): 169-198.

Fitzgerald, P., and Stump, E., 1992. Early Cretaceous uplift of the southern Sentinel Range, Ellsworth Mountains, West Antarctica. in Recent Progress in Antarctic Earth Science, Y. Yoshida, K. Kaminuma and K. Shiraishi (Editors), pp. 331-340, TERRAPUB, Tokyo.

Fretwell, P.,Pritchard, H.D.,Vaughan, D.G.,Bamber, J.L., Barrand, N.E., Bell, R., Bianchi, C., Bingham, R. G., Blankenship, D.D.,Casassa, G., Catania, G.,Callens, D.,Conway, H.,Cook, A.J.,Corr, H.F.J.,Damaske, D.,Damm, V.,Ferraccioli, F.,Forsberg, R.,Fujita, S.,Gim, Y.,Gogineni, P.,Griggs, J.A., Hindmarsh, R.C.A.,Holmlund, P.,Holt, J.W.,Jacobel, R.W., Jenkins, A.,Jokat, W.,Jordan, T.,King, E.C., Kohler, J.,Krabill, W.,Riger-Kusk, M., Langley, K.A., Leitchenkov, G.,Leuschen, C.,Luyendyk, B.P., Matsuoka, K.,Mouginot, J.,Nitsche, F.O.,Nogi, Y.,Nost, O.A.,Popov, S.V., Rignot, E.,Rippin, D.M., Rivera, A., Roberts, J.,Ross, N., Siegert, M.J.,Smith, A.M., Steinhage, D., Studinger, M.,Sun, B., Tinto, B.K.,Welch, B.C.,Wilson, D.,Young, D.A.,Xiangbin, C. and Zirizzotti, A., 2013. Bedmap2: improved ice bed, surface and thickness datasets for Antarctica. The Cryosphere, 7 (1): 375-393.

Galbraith, R., 1990: The Radial Plot: Graphical assessment of spread in ages. Nuclear Tracks and Radiation Measurements 17(3): 207-214.

Gohl, K., 2010. The Expedition of the Research Vessel “Polarstern” to the Amundsen Sea, Antarctica, in 2010 (ANT-XXVI/3); Berichte zur Polar- und Meeresforschung / Reports on Polar and Marine Research, 617, 173 pages, http://epic.awi.de/29635/.

Gohl, K., 2012. Basement control on past ice sheet dynamics in the Amundsen Sea Embayment, West Antarctica. Palaeogeography, Palaeoclimatology, Palaeoecology, 335-336: 35-41.

Gohl, K., Teterin, D., Eagles, G., Netzeband, G., Grobys, J., Parsiegla, N., Schlüter, P., Leinweber, V., Larter, R., Uenzelmann-Neben, G., Udintsev, G., 2007. Geophysical survey reveals tectonic structures in the Amundsen Sea embayment, West Antarctica. In Antarctica: A Keystone in a Changing World—Online Proceedings for the Tenth International Symposium on Antarctic Earth Sciences, eds. Cooper, A. K., C. R. Raymond et al., USGS Open-File Report 2007-1047, Short Research Paper 047, doi:10.3133/Of2007-1047.srp047.

Gohl, K., Denk, A., Wobbe, F. and Eagles, G., 2013a. Deciphering tectonic phases of the Amundsen Sea Embayment shelf, West Antarctica, from a magnetic anomaly grid, Tectonophysics, 585, 113-123.

Gohl, K., Uenzelmann-Neben, G., Larter, R.D., Hillenbrand, C.-D., Hochmuth, K., Kalberg, T., Weigelt, E., Davy, B., Kuhn, G. and Nitsche, F.-O., 2013b. Seismic stratigraphic record of the Amundsen Sea Embayment shelf from pre-glacial to recent times: Evidence for a dynamic West Antarctic ice sheet. Marine Geology, 344, 115-131.

Hillenbrand, C.-D., Kuhn, G., Smith, J. A., Gohl, K., Graham, A. G. C., Larter, R. D., Klages, J. P., Downey, R., Moreton, S. G., Forwick, M. and Vaughan, D. G., 2013. Grounding-line retreat of the West Antarctic Ice Sheet from inner Pine Island Bay. Geology 41, 35-38.

Holschuh, N., Pollard, D., Alley, R. and Anandakrishnan, S., 2014. Evaluating Marie Byrd Land stability using an improved basal topography. Earth and Planetary Science Letters 408, 362-369.

Ivany, L.C., Van Simaeys, S., Domack, E.W. and Samson, S.D., 2006. Evidence for an earliest Oligocene ice sheet on the Antarctic Peninsula. Geology, 34: 377-380.

Jenkins, A., Dutrieux, P., Jacobs, S.S., McPhail, S.D., Perrett, J.R., Webb, A.T. and White, D., 2010. Observations beneath Pine Island Glacier in West Antarctica and implications for its retreat. Nature Geoscience, 3: 468-472.

Johnson, J.S., Bentley, M.J. and Gohl, K., 2008. First exposure ages from the Amundsen Sea embayment, West Antarctica: the late Quaternary context for recent thinning of Pine Island, Smith and Pope Glaciers. Geology, 36: 223-226.

Jordan, T., Ferraccioli, F., Vaughan, D., Holt, J., Corr, H., Blankenship, D. and Diehl, T., 2010. Aerogravity evidence for major crustal thinning under Pine Island Glacier region (West Antarctica). Geological Society of America Bulletin, 122: 714-726.

748 Ketcham, R.A., 2005. Forward and inverse modeling of low-temperature thermochronometry data.
749 Reviews in Mineralogy and Geochemistry, 58: 275–314.

750 Ketcham, R.A., Carter, A., Donelick, R.A., Barbarand, J., and Hurford, A.J., 2007. Improved
751 modeling of fission-track annealing in apatite. American Mineralogist, 92 (5-6): 799-810.

752 Ketcham, R.A., Gautheron, C. and Tassan-Got, L., 2011. Accounting for long alpha-particle stopping
753 distances in (U–Th–Sm)/He geochronology: Refinement of the baseline case. Geochimica et
754 Cosmochimica Acta, 75 (24) 7779–7791.

755 Klages, J.P., Kuhn, G., Hillenbrand, C.-D., Grahan., A., Smith, J., Larter, R., Gohl, K., and Wacker, L.,
756 2014. Retreat of the West Antarctic Ice Sheet from the western Amundsen Sea shelf at a pre- or
757 early LGM stage. Quaternary Science Reviews 91, 1-15.

758 Korhonen, F., Saito, S., Brown, M., Siddoway, C., Day, J., 2010. Multiple generations of granite in the
759 Fosdick Mountains, Marie Byrd Land, West Antarctica. Implications for polyphase intracrustal
760 differentiation in a continental margin setting. Journal of Petrology 51, 627-670.

761 Larter, R.D., Cunningham, A.P., Barker, P.F., Gohl, K. and Nitsche, F.O., 2002. Tectonic evolution of
762 the Pacific margin of Antarctica 1. Late Cretaceous tectonic reconstructions. Journal of
763 Geophysical Research, 107 (B12): EPM 5-1 – EPM 5-19, doi: 10.1029/2000JB000052.

764 Larter, R. D., Anderson, J. B., Graham, A. G. C., Gohl, K., Hillenbrand, C.-D., Jakobsson, M.,
765 Johnson, J. S., Kuhn, G., Nitsche, F. O., Smith, J. A., Witus, A. E., Bentley, M. J., Dowdeswell, J.
766 A., Ehrmann, W., Klages, J. P., Lindow, J., Cofaigh, C. Ó., Spiegel, C., 2014. Reconstruction of
767 changes in the Amundsen Sea and Bellingshausen Sea sector of the West Antarctic Ice Sheet
768 since the Last Glacial Maximum. Quaternary Science Reviews 100, 55-86, doi:
769 http://dx.doi.org/10.1016/j.quascirev.2013.10.016.

770 Lawver, L. A. and Gahagan, L.M., 1994. Constraints on the timing of extension in the Ross Sea region.
771 Terra Antartica, 1: 545-552.

772 LeMasurier, W. E., 1972. Volcanic record of Cenozoic glacial history of Marie Byrd Land, Antarctic
773 Geology and Geophysics (R. J. Adie ed), 251–260, Universitetsforlaget, Oslo, 1972.

774 LeMasurier, W.E., 2006: What supports the Marie Byrd Land Dome? An evaluation of potential uplift
775 mechanisms in a continental rift system. In Fütterer, D.K., Damaske, D., Kleinschmidt, G., Miller,
776 H. and Tessensohn, F. (eds.), Antarctica: Contributions to global earth sciences. Berlin,
777 Heidelberg, New York: Springer-Verlag, 299 302.

778 LeMasurier, W. E. 2008. Neogene extension and basin deepening in the West Antarctic rift inferred
779 from comparisons with the East African rift and other analogs. Geology 36 (3): 247-250,
780 doi:10.1130/G24363A.1.

781 LeMasurier, W.E., Rex, D.C., 1989. Evolution of linear volcanic ranges in Mary Byrd Land, West
782 Antarctica. Journal of Geophysical Research 94, 7223-7236.

783 LeMasurier, W. E. and C. A. Landis. 1996. Mantle-plume activity recorded by low relief erosion
784 surfaces in West Antarctica and New Zealand. Bulletin of the Geological Society of America 108:
785 1450-1466.

786 Lindow, J., 2014. Fire and Ice – Tectonic and glacial history of the Amundsen Sector, West Antarctica.
787 Ph.D. thesis, University of Bremen, 161 pp.

788 Lindow, J., Castex, M., Wittmann, H., Johnson, J., Lisker, F., Gohl, K. and Spiegel, C., 2014. Glacial
789 retreat in the Amundsen Sea sector, West Antarctica – first cosmogenic evidence from central
790 Pine Island Bay and the Kohler Range. Quaternary Science Reviews 98: 166-173.

791 Lippolt, H.J., Leitz, M., Wernicke, R.S. and Hagedorn, B., 1994. (Uranium + thorium)/helium dating
792 of apatite: experience with samples from different geochemical environments. Chemical Geology,
793 112 (1-2): 179-191.

794 Lisker, F., 2002. Review of fission track studies in northern Victoria Land – Passive margin evolution
795 versus uplift of the Transantarctic Mountains. - Tectonophysics, 349 (1-4): 57-73.

796 Lisker, F. and Olesch, M., 1998. Cooling and denudation history of western Marie Byrd Land,
797 Antarctica, based on apatite fission-tracks. - In: Van den haute, P. & De Corte, F. (eds.),
798 Advances in fission-track geochronology, Kluwer Academic Publishers, Dordrecht: 225-240.

799 Lopatin, B.G. and Orlenko, E.M., 1972. Outline of the geology of Marie Byrd Land and Eights Coast.
800 In: Antarctic Geology and Geophysics (R. J. Adie.- ed.). Oslo, Universitetsforlaget. 245-250.

801 Miller, K.G., Wright, J.D. and Fairbanks, R.G., 1991. Unlocking the Ice House: Oligocene–Miocene
802 oxygen isotopes, eustasy, and margin erosion. Journal of Geophysical Research, 96: 6829–6848.

803 Müller, R.D., Gohl, K., Cande, S.C., Goncharov, A. and Golynsky, A.V., 2007. Eocene to Miocene
804 geometry of the West Antarctic rift system. Australian Journal of Earth Sciences 54, 1033-1045.

805 Mukasa, S. and Dalziel, I., 2000. Marie Byrd Land, West Antarctica: Evolution and Gondwana´s
806 Pacific margin constrained by zircon U-Pb geochronology and feldspar common-Pb isotopic
807 compositions. Geological Society of America Bulletin, 112: 611-627.

808 Naish, T., Powell, R., Levy, R., Wilson, G., Scherer, R., Talarico, F., Krissek, L., Niessen, F.,
809 Pompilio, M.,Wilson, T., Carter, L., DeConto, R., Huybers, P., McKay, R., Pollard, D., Ross, J.,
810 Winter, D., Barrett, P., Browne, G., Cody, R., Cowan, E., Crampton, J., Dunbar, G., Dunbar, N.,
811 Florindo, F., Gebhardt, C., Graham, I., Hannah, M., Hansaraj, D., Harwood, D., Helling, D.,
812 Henrys, S., Hinnov, L., Kuhn, G., Kyle, P., Läufer, A., Maffioli, P., Magens, D., Mandernack, K.,
813 McIntosh, W., Millan, C., Morin, R., Ohneiser, C., Paulsen, T., Persico, D., Raine, I., Reed, J.,
814 Riesselman, C., Sagnotti, L., Schmitt, D., Sjunneskog, C., Strong, P., Taviani, M., Vogel, S.,
815 Wilch, T. and Williams, T. 2009: Obliquity-paced Pliocene West Antarctic ice sheet oscillations.
816 Nature, 458: 322-329.

817 Pankhurst, R.J., Weaver, S.D., Bradshaw, J.D., Storey, B.C. and Ireland, T.R., 1998. Geochronology
818 and geochemistry of pre-Jurassic superterranes in Marie Byrd Land, Antarctica. Journal of
819 Geophysical Research 103:2529-2547.

820 Payne, A.J., Vieli, A., Shepherd, A.P., Wingham, D.J. and Rignot, E., 2004. Recent dramatic thinning
821 of largest West Antarctic ice stream triggered by oceans. Geophysical Research Letters, 31,
822 L23401, doi:10.1029/2004GL021284.

823 Pollard, D. and DeConto, R.M., 2009. Modelling West Antarctic ice sheet growth and collapse
824 through the past five million years. Nature, 458, doi:10.1038/nature07809.

825 Prenzel, J., Lisker, F., Elsner, M., Schöner, R., Balestrieri, M.L., Läufer, A., Berner, U. and Spiegel,
826 C., 2014. Burial and exhumation of the Eisenhower Range, Transantarctic Mountains, based on
827 thermochronology, maturity and sediment petrographic constraints. Tectonophysics 630, 113-130.

828 Prenzel, J., Lisker, F., Balestrieri, M.L., Läufer, A. and Spiegel, C., 2013. The Eisenhower Range,
829 Transantarctic Mountains: Evaluation of qualitative interpretation concepts of
830 thermochronological data. Chemical Geology, 352: 176-187.

831 Pritchard, H.D., Arthern, R.J., Vaughan, D.G. and Edwards, L.A., 2009. Extensive dynamic thinning
832 on the margins of the Greenland and Antarctic ice sheets. Nature, 461, doi:10.1038/nature08471

833 Richard, S.M., Smith, C.H., Kimbrough, D.L., Fitzgerald, P.G., Luyendyk, B.P., and McWilliams,
834 M.O., 1994. Cooling history of the northern Ford Ranges, Marie Byrd Land, West Antarctica.
835 Tectonics, 13 (4): 837-857.

836 Rignot, E., Bamber, J.L., van den Broeke, M.R., Davis, C., Li, Y., van de Berg, W.J. and van
837 Meijgaard, E., 2008. Recent Antarctic ice mass loss from radar interferometry and regional
838 climate modelling. Nature Geoscience, 1: 106-110, doi:10.1038/ngeo102.

839 Rignot, E., Mouginot, J., Morlighem, M., Seroussi, H. and Scheuchl, B., 2014. Widespread, rapid
840 grounding line retreat of Pine Island, Thwaites, Smith, and Kohler glaciers, West Antarctica, from
841 1992 to 2011. Geophysical Research Letters, 41 (10): 3502–3509, doi:10.1002/2014GL060140.

Rocchi, S., LeMasurier, W., Di Vicenzo, G., 2006: Oligocene to Holocene erosion and glacial history in Marie Byrd Land, West Antarctica, inferred from exhumation of the Dorrel rock intrusive complex and from volcano morphologies. Geological Society of America Bulletin, 118: 991-1005.

Ross, N., Siegert, M. J., Woodward, J., Smith, A. M., Corr, H. F. J., Bentley, M. J., Hindmarsh, R. C. A., King, E. C. and Rivera, A., 2011. Holocene stability of the Amundsen-Weddell ice divide, West Antarctica. Geology 39, 935-938.

Schroeder, D.M., Blankenship, D.D., Young, D.A. and Quartini, E., 2014. Evidence for elevated and spatially variable geothermal flux beneath the West Antarctic Ice Sheet. PNAS, 111 (25): 9070–9072.

Siddoway, C.S, Richard, S., Fanning, C.M. and Luyendyk, B.P., 2004. Origin and emplacement mechanisms for a middle Cretaceous gneiss dome, Fosdick Mountains, West Antarctica, in Whitney, D.L., Teyssier, C.T., and Siddoway, C., eds., Gneiss domes in orogeny, GSA Special Paper 380: 267-294.

Siddoway, C., 2008. Tectonics of the West Antarctic rift system: New light on the history and dynamics of distributed intracontinental extension in Cooper, A.K., P.J. Barrett, H.Stagg, B.Storey, E.Stump, W.Wise, and the 10th ISAES editorial team (eds.), Antarctica: A Keystone in a Changing World, Proceedings of the 10th International Symposium on Antarctic Earth Sciences. Washington, DC: The National Academies Press, p. 91-114.

Spiegel, C., Kohn, B., Raza, A., Rainer, T. and Gleadow, A., 2007. The effect of long-term low-temperature exposure on apatite fission track stability: a natural annealing experiment in the deep ocean. Geochimica et Cosmochimica Acta 71, 4512-4537.

Spiegel, C., Kohn, B., Belton, D., Berner, Z. and Gleadow, A., 2009. Apatite (U-Th-Sm)/He thermochronology of rapidly cooled samples: the effect of He implantation. Earth and Planetary Science Letters 285, 105-114.

Storti, F., Balestrieri, M.L., Balsamo, F. and Rossetti, F., 2008. Structural and thermochronological constraints to the evolution of the West Antarctic Rift System in central Victoria Land. Tectonics, 27, TC4012, doi: 10.1029/2006TC002066.

Sutherland, R., 1999. Basement geology and tectonic development of the greater New Zealand region: An interpretation from regional magnetic data. Tectonophysics, 308: 341-362.

Tagami, T., Shimada, C., 1996. Natural long-term annealing of the zircon fissin track system around a granitic pluton. Journal of Geophysical Research 101, 8245-8255.

Tessensohn, F. and Wörner, G., 1991. The Ross Sea Rift System: Structure, evolution and analogues. In Geological Evolution of Antarctica, eds. M. R. A. Thomson, J. A. Crame, and J. W. Thomson., Cambridge, Cambridge University Press: pp. 273-277.

Van der Veen, C., Leftwich, T., von Frese, R., Csatho, B. and , Li, J., 2007. Subglacial topography and geothermal heat flux: Potential interactions with drainage on the Greenland ice sheet. Geophysical Research Letters 34, L12501.

Wagner, G.A., 1972. The geological interpretation of fission track ages. Transaction of the American Nuclear Society, 15 (1): 117.

Wagner, G.A., Gleadow, A.J.W. and Fitzgerald, P.G. 1989. The significance of the partial annealing zone in apatite fission-track analysis: Projected track length measurements and uplift chronology of the transantarctic mountains. Chemical Geology Isotope Geoscience Section, 79 (4): 295-305. doi:10.1016/0168-9622(89)90035-3

Wilson, D.S., Jamieson, S.S.R., Barrett, P.J., Leitchenkov, G., Gohl, K. and Larter, R.D., 2012. Antarctic topography at the Eocene-Oligocene boundary. Palaeogeography, Palaeoclimatology, Palaeoecology, 335-336: 24-34.

Wilson, D.S., Pollard, D., DeConto, R.M., Jamieson, S.S.R.and Luyendyk, B.P. 2013. Initiation of the West Antarctic Ice Sheet and estimates of total Antarctic ice volume in the earliest Oligocene. Geophysical Research Letters, 40: 4305–4309.

Wolf, R.A., Farley, K.A. and Kass, D.M., 1998. Modelling of the temperature sensitivity of the apatite (U–Th)/He thermochronometer. Chemical Geology, 148: 105–114.

Zachos, J. C., Breza, J. and Wise, S.W. 1992. Early Oligocene ice-sheet expansion on Antarctica: stable isotope and sedimentological evidence from Kerguelen Plateau, southern Indian Ocean. Geology 20: 569-573.

Zachos, J., Pagani, M., Sloan, L., Thomas, E., Billups, K., 2001. Trends, rhythms, and abberations in global climate 65 Ma to present. Science 292, 686-693.

Zattin, M., Pace, D., Andreucci, B., Rossetti, F. and Talarico, F., 2014. Cenozoic erosion of the Transantarctic Mountains. A source-to-sink thermochronological study. Tectonophysics 630, 158-165.

Zeitler, P., Herczeg, A., McDougall, I., Honda, M., 1987. U-Th-He dating of apatite: a potential thermochronometer. Geochimica et Cosmochimica Acta 51, 2865-2868.

APPENDIX – Analytical details for thermochronological dating methods

A1:Fission track thermochronology

For each sample, between ~3 and 10 kg of rock was collected from the field. Apatite and zircon crystals were separated from the rocks by crushing, sieving, Wilfley table, magnetic and heavy liquid separation techniques. Samples with MB laboratory codes were processed and dated in the fission track laboratory of the University of Waikato, New Zealand; those with MBL and PS laboratory codes in the thermochronology laboratory of the University of Bremen, Germany. As kinetic indicator, we used the bulk etching velocity of apatite expressed by the size of etch pit diameters parallel to the crystallographic c-axis (= Dpar value; Donelick, 1993; Burtner et al., 1994). Due to the anisotropy of apatite, track annealing also depends on the position of the track within the apatite crystal, which is why the angle of each measured track length relative to the c-axis is determined (Ketcham et al., 2007). All lengths and Dpar measurements were carried out in the Bremen laboratory.

Apatite grains were embedded in epoxy resin, grinded and polished to reveal internal surfaces, and etched with 5 M HNO_3 for 20 seconds at 20°C (Bremen) and 21°C (Waikato). Zircon was embedded in Teflon, grinded and polished, and etched in a NaOH-KOH eutectic melt at 230 ± 1°C for 20 hours (Waikato). Thermal neutron irradiations for the Bremen samples were carried out at the Garching FRM II reactor facility in Germany, and for the Waikato samples at the ANSTO reactor facility at

922 Lucas Heights, Sidney, Australia. Fission track ages were measured using the external detector method
923 and the zeta calibration approach (Gleadow, 1981, Hurford and Green, 1983, respectively), with a zeta
924 for zircon fission track dating of 135 ± 3 (CN1 dosimeter glass, Waikato), and a zeta for apatite fission
925 track dating of 344 ± 5 (SRM 612 dosimeter glass, Waikato) and 324 ± 11 (CN5 dosimeter glass,
926 Bremen).

927 External mica detectors were etched in 40% HF for 25 minutes at room temperature. Each apatite
928 grain analysed for track lengths or age was additionally analysed for etch pit size (Dpar). Dpar values
929 were measured by averaging 3 – 4 measurements for each grain. No track lengths or kinematic
930 indicators were measured for zircon fission track analysis. Track densities, lengths and Dpar values
931 were measured using a Zeiss Axioplan with 1000 x magnification. Central ages and error limits were
932 calculated using the software TRACKKEY, version 4.2.g (Dunkl, 2002).

933 Generally, we tried to date up to 20 grains and measure up to 100 track lengths for AFT analysis,
934 although due to apatite yield and sample quality this was not possible for every sample. For analysing
935 the detrital samples from the Wrigley Gulf, we dated up to 80 grains, corresponding to >95%
936 confidence that no fraction ≥ 0.085 is missed (Vermeesch, 2004). From the resulting age distributions,
937 single-grain age groups are derived using the binomial peak fitting method (Brandon, 1992). To
938 determine the optimal number of age groups, the F-test is applied. P(F) gives the probability that
939 random variation alone could produce the observed statistics. P(F) < 5% is considered to indicate that
940 the improvement in fit by adding a further age group is significant (Brandon, 1992, 2002)

941

942 **A2: Apatite (U-Th-Sm)/He thermochronology**

943 Grains for apatite (U-Th-Sm)/He analysis were handpicked from the mineral separates. Only pristine
944 grains without cracks, inclusion, broken surfaces, and with grain radii >50 µm were chosen. Selected
945 grains were measured for grain dimensions, classified according to grain morphology, and
946 photographically documented. Grains were then mounted in platinum capsules, which were previously
947 cleaned with 37% HCl at 35-40°C for 48 h. Measurement of He, U, Th, and Sm were performed at the

University of Melbourne, Australia. Helium was extracted from apatite crystals by laser heating (10 minutes, 920°C) using a solid-state diode laser (820 nm wavelength, fibre-optic coupling). The extracted helium was measured by the ^{3}He isotope dilution method using a Balzers quadrupole mass spectrometer. Afterwards, apatites were retrieved from the laser chamber, dissolved in 5% HNO_3, and measured for U, Th, and Sm contents using a second-generation Varian quadrupole ICP-MS. Reference material BHVO-1 (Eggins et al., 1997) was used as a calibration standard, and in-house standard Mud Tank apatite and international rock standard BCR-2 were used as additional internal standards. Accuracy and precision of U, Th, and Sm measurements range up to 2% (at $\pm 2\sigma$), but is typically better than 1% at Melbourne University. Apatite (U-Th-Sm)/He ages were calculated using a Bremen-group internal Microsoft Excel spreadsheet based on the ^{4}He ingrowth equation (e.g., Farley, 2002) and the first-order Taylor series approximation (Taylor, 1969). Calculated raw ages were corrected for alpha-ejection after Farley et al. (1996). The calculation includes an analytical error of ~5% combining laboratory internal analytical uncertainties, errors related to grain size measurements and alpha ejection correction. Radiogenically-derived ^{4}He travels ca. 20 µm through the apatite crystal before it comes to rest (= stopping distance; Farley et al., 1996), which is why the outer rim of the crystal becomes He-depleted. Accordingly, each measured AHe age is corrected for this alpha-ejection effect, based on morphology and size of the analyzed grain (Farley et al., 1996). Since our AHe dates show no correlation with effective U-concentration, we assume that the AHe data are not influenced by radiation damage effects.

For integrating AFT and AHe ages (and for two samples with ZFT ages as well), we used thermal history inversions. These are based on algorithms that describe track annealing and He diffusion as observed from laboratory experiments calibrated to geological timescales. Using a Monte Carlo simulation, between 10000 and 100000 thermal histories are tested against the observed data, thereby revealing a range of thermal histories that are statistically in good or acceptable agreement with the data (defined as goodness of fit values of 0.5 and 0.05, respectively; Ketcham, 2005). A “good” result can be interpreted as a time-temperature path supported by the measured data, while an acceptable path is not ruled out by the input data (Ketcham, 2005).

975

976 **References**

977 Brandon, M.T., 1992. Decomposition of fission-track grain-age distributions. American Journal of
978 Science, 292: 535–564.

979 Brandon, M.T., 2002. Decomposition of mixed grain age distributions using Binomfit. On Track, 24:
980 13–18.

981 Burtner R.L., Nigrini A. and Donelick R.A., 1994. Thermochronology of Lower Cretaceous source
982 rocks in the Idaho-Wyoming thrust belt. AAPG Bulletin, 78 (10): 1613–1636.

983 Donelick R., 1993. Apatite etching characteristics versus chemical composition. Nuclear Tracks and
984 Radiation Measurements, 21 (4): 604.

985 Dunkl, I., 2002. Trackkey: a Windows program for calculation and graphical presentation of fission
986 track data. Computer and Geosciences 28, 3-12.

987 Eggins, S., Woodhead, J., Kinsley, L., Mortimer, G., Sylvester, P., McCulloch, M., Hergt, J., Handler,
988 M., 1997. A simple method for the precise determination of > 40 trace elements in geological
989 samples by ICPMS using enriched isotope internal standardisation. Chemical Geology 134,
990 311-326.

991 Farley, K., 2002. (U-Th)/He Dating: Techniques, calibrations, and applications. Reviews in
992 Mineralogy and Geochemistry 47, 819-844.

993 Farley, K., Wolf, R., Silver, L., 1996. The effects of long alpha-stopping distances on (U-Th)/He ages.
994 Geochimica et Cosmochimica Acta 60, 4223-4229.

995 Gleadow, A., 1981. Fission track dating methods: what are the real alternatives? Nuclear Tracks and
996 Radiation Measurements 5, 3-14.

997 Hurford, A., Green, P., 1983. The zeta age calibration of fission track dating. Chemical Geology 41,
998 285-317.

999 Ketcham, R.A., 2005. Forward and inverse modeling of low-temperature thermochronometry data.
1000 Reviews in Mineralogy and Geochemistry, 58: 275–314.

1001 Ketcham, R.A., Carter, A.C., Donelick, R.A., Barbarand, J. and Hurford, A.J., 2007. Improved
1002 measurement of fission-track annealing in apatite using c-axis projection. American
1003 Mineralogist, 92: 789–798.

1004 Taylor, B., 1969. Proposition VII, Theorem 3, Corollary 2, Methodus Incrementorum Directa et
1005 Inversa [Direct and reverse methods of incrementation] (London, 1715). Harvard University
1006 Press, Cambridge, Massachusetts, pp 329-332.

1007 Vermeesch, P., 2004. How many grains are needed for a provenance study? Earth and Planetary
1008 Science Letters, 224 (3-4): 441–451.

1009

1010

1011 **Figure Captions**

1012 **Fig 1**: Subglacial topography of the West Antarctic Rift System (data from Bedmap2, Fretwell et al.,

1013 2013). Thick white lines delineate crustal blocks that constitute West Antarctica (after Dalziel and

1014 Elliot, 1982). Dotted lines show location of proposed rift branches, open circles refer to sample

locations. Abbreviations: AP – Antarctic Peninsula, AS – Amundsen Sea, BS – Bellingshausen Sea, EWM – Ellsworth Whitmore Mountains, FR – Ferrigno Rift (Bingham et al., 2012), HC – Hobbs Coast, KR – Kohler Range, MBL – Marie Byrd Land, MM – Mount Murphy, PIB – Pine Island Bay (location of samples studied by Lindow, 2014), PIR – Pine Island Rift (Jordan et al., 2010), RS – Ross Sea, TAM – Transantarctic Mountains, TI – Thurston Island, WARS – West Antarctic Rift System, WG – Wrigley Gulf.

Fig. 2: Geological map of eastern Marie Byrd Land after Lopatin and Orlenko (1974), modified and complemented by data from Brand (1979), Pankhurst et al. (1998), Mukasa and Dalziel (2000), and Rocchi et al. (2006). Ages of Cenozoic volcanoes are after LeMasurier and Rex (1989). Names of nunataks sampled for this study are marked in red. Dashed boxes outline areas shown in Fig. 3.

Fig. 3: Detailed view of the study area and sample locations. Grey-shaded areas outline mountain ranges, magenta-coloured areas refer to rock exposures. For position within Marie Byrd Land see Fig. 2. **3A**: Samples from the Kohler Range and the Mt. Murphy area. Sketch is based on the 1:500 000 topographic map "Bakutis Coast – Marie Byrd Land" compiled by the US Geological Survey in 1966. **3B**: Samples from the Hobbs Coast / Demas Range. Sketch is based on the 1:500 000 topographic map "Hobbs Coast – Marie Byrd Land", compiled by the US Geological Survey in 1965.

Fig. 4: Bathymetry of the western Wrigley Gulf (Fig. 1) after Klages et al. (2014) with locations of box core samples as well as lithological compositions of the three box cores, based on the petrographic analysis of clasts >2 mm.

Fig. 5: Radial Plot (Galbraith, 1990), showing the results of AFT analysis from box cores PS75/130-2 and PS75/133-1 (Wrigley Gulf). Each box core contained two age groups, reflecting the cooling history integrated over the catchment area of the Berry Glacier. Data deconvolution and F-test after Brandon (1992 & 2002).

Fig. 6: Thermal history inversions of samples from eastern Marie Byrd Land, integrating apatite fission track and (U-Th-Sm)/He thermochronology. Inversions are based on Monte Carlo simulations with 10 000 to 100 000 paths. Dark and light-grey envelopes comprise thermal histories in good and

1041 acceptable agreement with the data observed, corresponding to goodness of fit values of 0.5 and 0.05.
1042 Thick black lines refer to the weighted mean paths (calculated from the good and acceptable fits and
1043 weighted according to the goodness-of-fit values; Ketcham, 2005). Also shown are the temperature
1044 ranges to which the applied dating methods are most sensitive (40 to 85°C for apatite (U-Th-Sm)/He
1045 and 60 to 120°C for apatite fission track thermochronology). The samples from the Mt. Murphy area
1046 experienced rapid cooling at ~30 Ma (pink dashed line). The other samples show rapid cooling during
1047 the late Cretaceous, followed by slow cooling and renewed rapid cooling at ~20 Ma (except for the
1048 Wunneburger Rock sample). The latest, post-20 Ma cooling episode (orange dashed line) is best
1049 defined by the tightly constrained sample MBL-51-10.

1050 **Fig. 7**: Compilation of weighted mean paths from different areas of eastern Marie Byrd Land (taken
1051 from Fig. 6), with interpretations regarding the tectonomorphic evolution. Numbers refer to sample
1052 elevations. Shades of grey indicate the temperature range of the fission track partial annealing zone
1053 (120 to 60°C), the He partial retention zone (85 to 40°C) and their overlap (85 to 60°).

1054 **Fig. 8:** Structural interpretation of data from this study (marked in red and blue) reconciling the
1055 thermochronology data with subglacial topography and with previously published structural data.
1056 Thick dashed blue line: Fault separating Wunneburger Rock from the Kohler Range, presumably
1057 active during late Cretaceous continental breakup. Thick dashed red lines: Faults delineating horst-
1058 and-graben structures adjacent to the Mt. Murphy Rift (MMR), active since the early Oligocene. The
1059 extension of the Mt. Murphy Rift cuts the Byrd Subglacial Basin, causing it to bend towards the north
1060 / Amundsen Sea Embayment. The Ferrigno Rift may extend into the Bentley Subglacial Trench
1061 (Bingham et al., 2012). If our model is valid, it would also explain the oblique geometries of the
1062 Ferrigno Rift, as compared with the Pine Island Rift, and of the Bentley Trough, as compared to the
1063 Byrd Subglacial Basin. Based on facts (i.e., on thermochronology data) is the existence of two fault
1064 structures separating the Mt. Murphy block from the surrounding areas (dashed red lines), and the
1065 activity of these fault structures since early Oligocene. The exact positions of the two faults are only
1066 weakly constrained, and are inferred from geomorphology and from field observations by LeMasurier
1067 (1972). Early Cenozoic dextral transtension along the Ferrigno Rift area was previously suggested by

Müller et al. (2007). Sinistral transtension along the Mt. Murphy Rift is based on assumptions and yet to be proven. Subglacial topography is from Fretwell et al. (2013; Bedmap2). Abbreviations: AP – Antarctic Peninsula, AS – Amundsen Sea, BS – Bellingshausen Sea, BSB – Byrd Subglacial Basin, BT – Bentley Subglacial Trench, EWM – Ellsworth Whitmore Mountains, FR – Ferrigno Rift (Bingham et al., 2012), HC – Hobbs Coast, KR – Kohler Range, MBL – Marie Byrd Land, MM – Mount Murphy, PIB – Pine Island Bay (location of samples studied by Lindow, 2014), PIR – Pine Island Rift (Jordan et al., 2010), RS – Ross Sea, TAM – Transantarctic Mountains, TI – Thurston Island, WARS – West Antarctic Rift System, WG – Wrigley Gulf, WR - Wunneburger Rock.

Fig. A1: Clasts from box cores of the Wrigley Gulf, representing lithologies subglacially exposed within the catchment area of the Berry Glacier. **5A**: Quartz-Monzonite deformed at the brittle-ductile transition, containing greenish pseudotachylite veins. PS75/132-1. **5B:** Greenish rhyolite, containing perfectly euhedral quartz crystals (dark spots). PS75/133-1. **5C**: Light-coloured granite containing small euhedral garnets. Similar rocks are exposed onshore at the Mount Goorhigian, forming part of the Demas Range migmatite complex (Mukasa and Dalziel, 2000). PS75/133-1. **5D**: Coarse-grained basic granulite, containing large garnet crystals. PS75/133-1. **5E & F**: Green low-grade meta-sedimentary rocks which probably represent equivalents to the Swanson Formation of the Ford Range (western Marie Byrd Land). PS75/130-2 & 133-1. **5G & H**: Semi-lithified clastic sediments containing volcanic and plutonic lithic fragments. They may also be of glaciomarine origin, i.e., formed in-situ in the Wrigley Gulf. PS75/133-1.

Fig. A2: Age elevation relationships for AFT (squares) and AHe (circles) samples from the Mt. Murphy area, the Hobbs Coast and the Kohler Range.

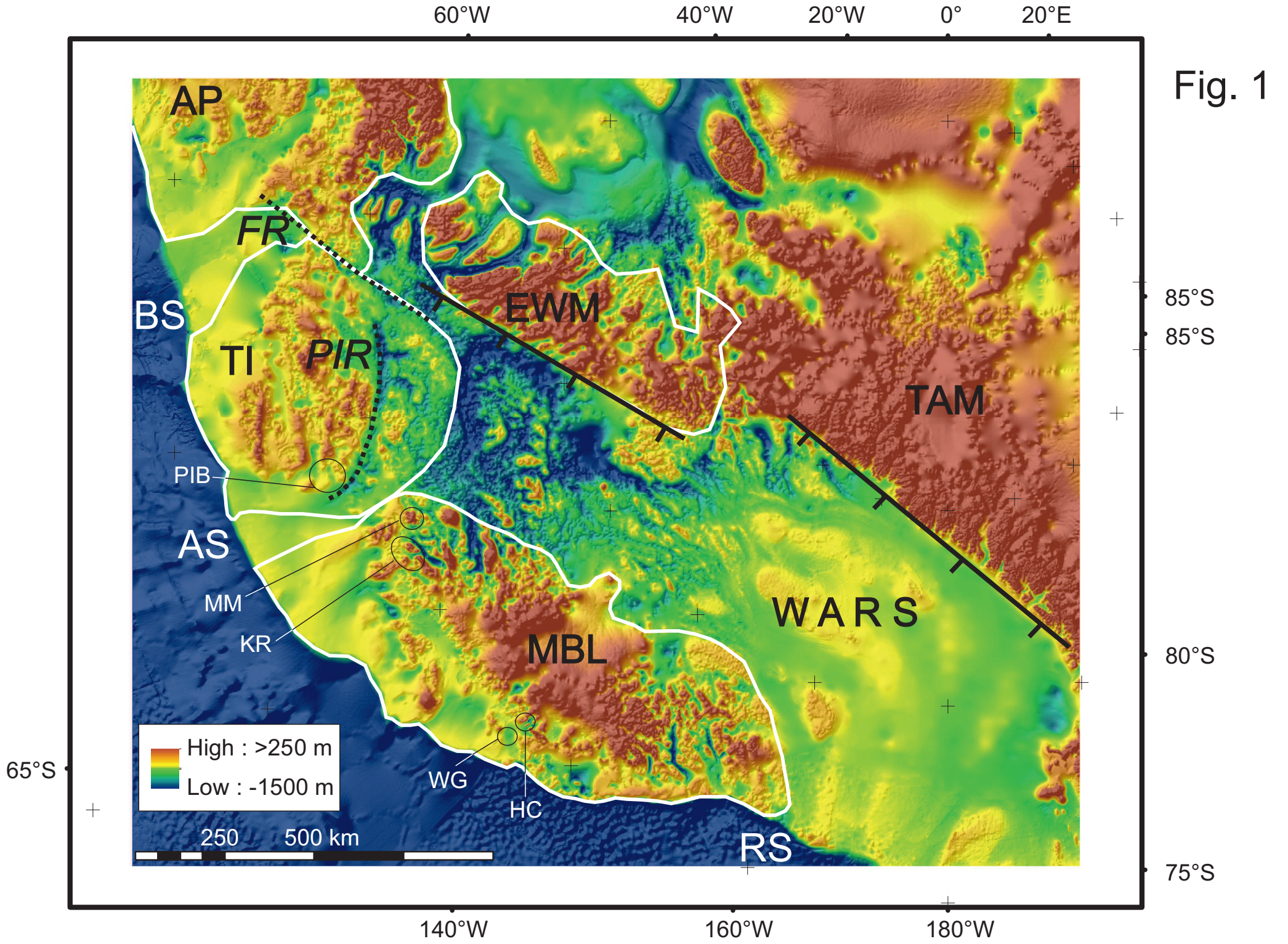
60°W
40°W
20°W
0°
20°E
85°S
85°S
80°S
75°S
65°S
140°W
160°W
180°W
AP
FR
BS
TI
PIR
EWM
TAM
PIB
AS
MM
KR
MBL
WARS
WG
HC
RS
High : >250 m
Low : -1500 m
250
500 km

Fig. 1

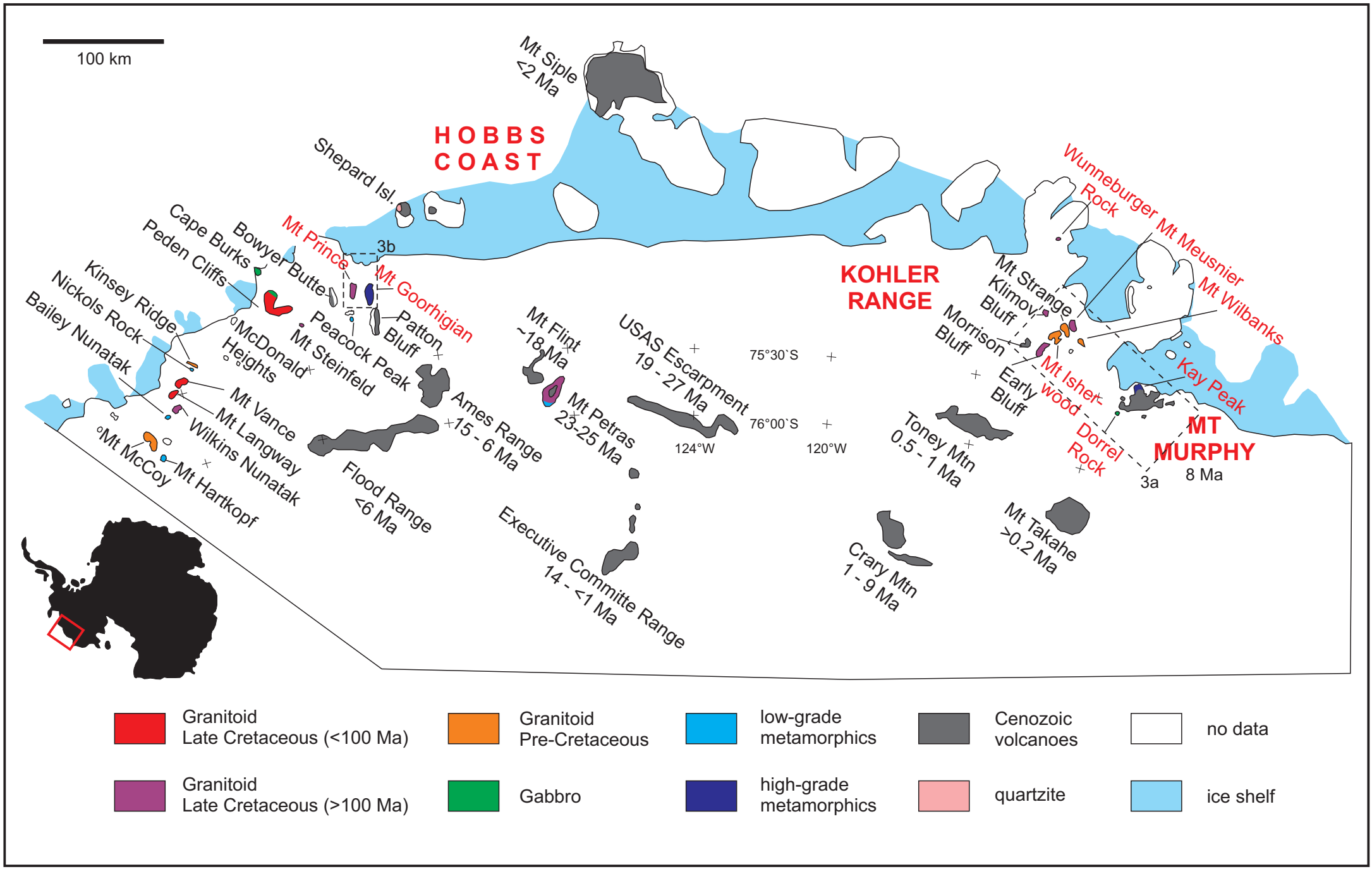
100 km
Mt Siple
<2 Ma
HOBBS
COAST
Shepard Isl.
Mt Prince
3b
Mt Goorhigian
Cape Burks
Bowyer Butte
Peden Cliffs
Kinsey Ridge
Nickols Rock
Bailey Nunatak
McDonald
Heights
Mt Steinfeld
Peacock Peak
Patton
Bluff
Mt Vance
Mt Langway
Wilkins Nunatak
Mt McCoy
Mt Hartkopf
Ames Range
15 - 6 Ma
Flood Range
<6 Ma
Mt Flint
~18 Ma
Mt Petras
23-25 Ma
USAS Escarpment
19 - 27 Ma
124°W
75°30`S
76°00`S
120°W
Executive Committe Range
14 - <1 Ma
KOHLER
RANGE
Crary Mtn
1 - 9 Ma
Toney Mtn
0.5 - 1 Ma
Mt Takahe
>0.2 Ma
Morrison
Bluff
Mt Strange
Klimov
Bluff
Early
Bluff
Mt Ishe-
wood
Dorrel
Rock
3a
Wunneburger
Rock
Mt Meusnier
Mt Wilbanks
Kay Peak
MT
MURPHY
8 Ma
Granitoid
Late Cretaceous (<100 Ma)
Granitoid
Late Cretaceous (>100 Ma)
Granitoid
Pre-Cretaceous
Gabbro
low-grade
metamorphics
high-grade
metamorphics
Cenozoic
volcanoes
quartzite
no data
ice shelf

Fig. 2

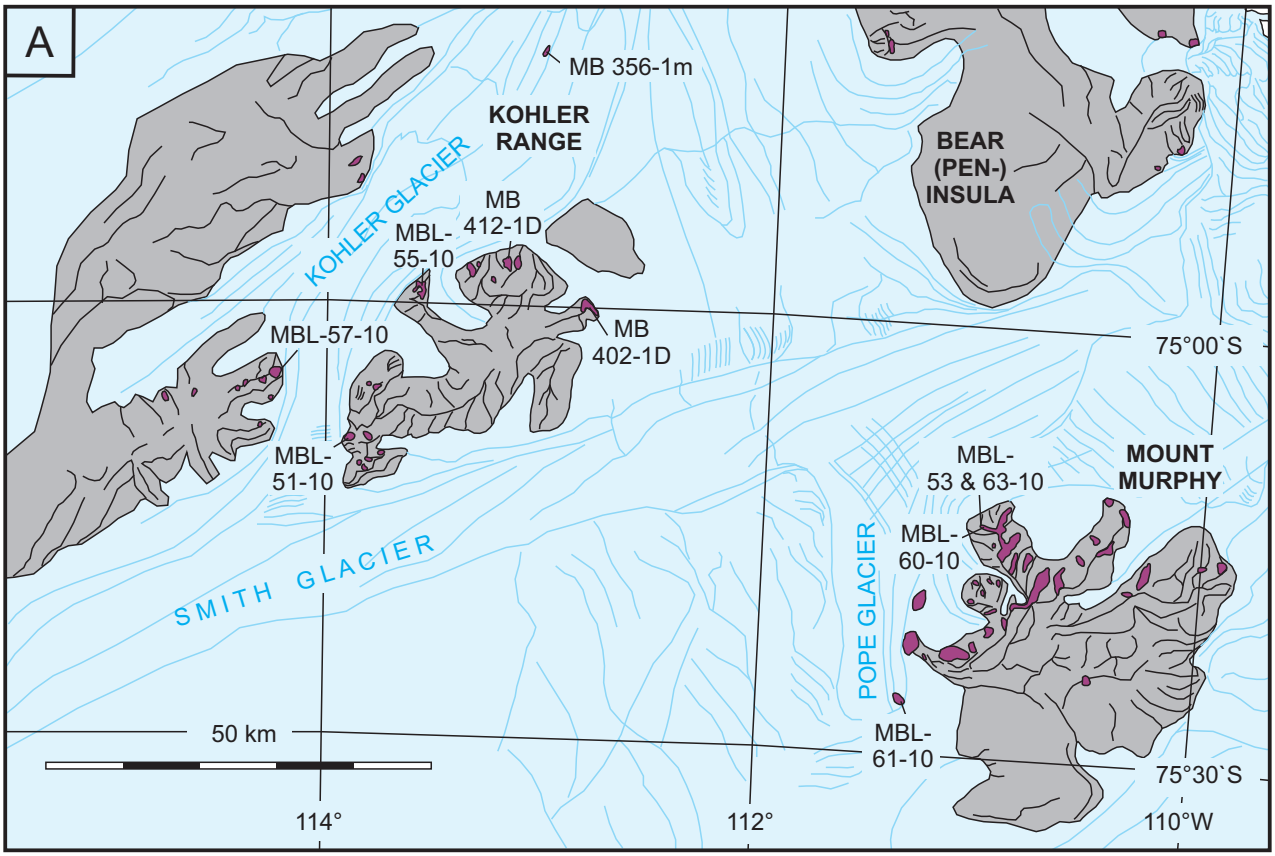
A
MB 356-1m
KOHLER RANGE
KOHLER GLACIER
MB 412-1D
MBL-55-10
MB 402-1D
MBL-57-10
MBL-51-10
SMITH GLACIER
BEAR (PEN-) INSULA
75°00`S
MBL-53 & 63-10
MOUNT MURPHY
POPE GLACIER
MBL-60-10
MBL-61-10
75°30`S
50 km
114°
112°
110°W

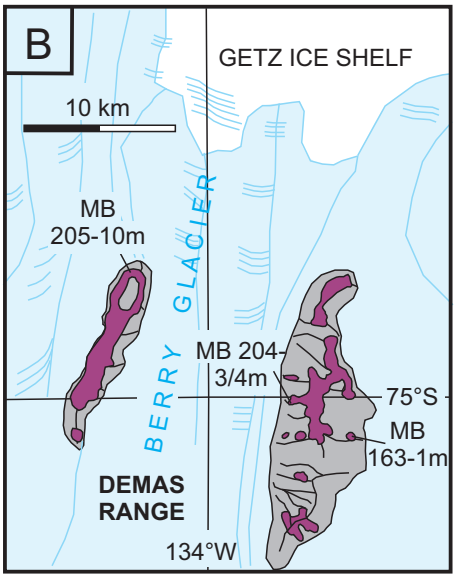
B
GETZ ICE SHELF
10 km
MB 205-10m
BERRY GLACIER
MB 204-3/4m
75°S
MB 163-1m
DEMAS RANGE
134°W

Fig. 3

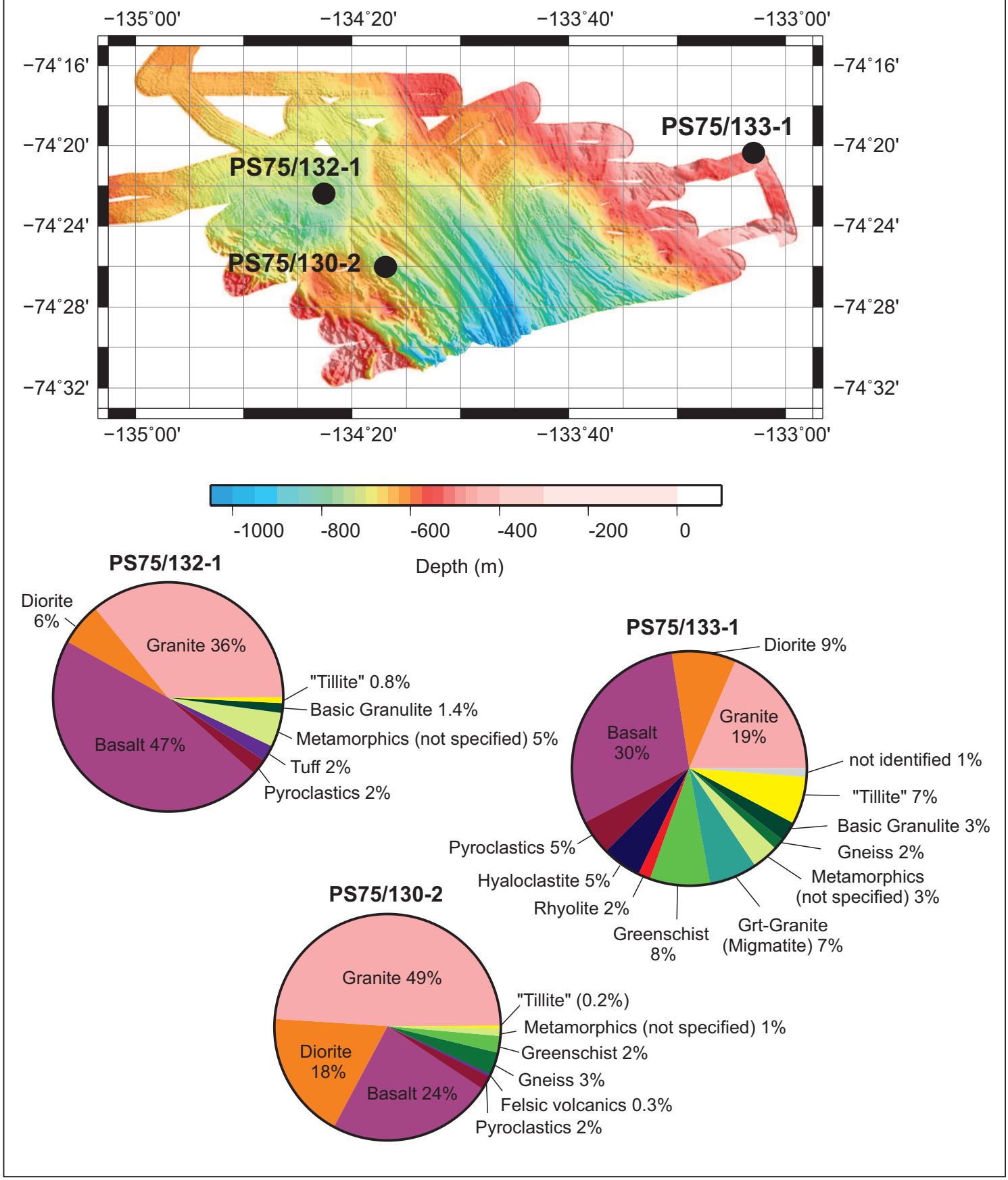
−135˚00'
−134˚20'
−133˚40'
−133˚00'
−74˚16'
−74˚20'
−74˚24'
−74˚28'
−74˚32'
PS75/132-1
PS75/133-1
PS75/130-2
-1000
-800
-600
-400
-200
0
Depth (m)
PS75/132-1
Diorite 6%
Granite 36%
"Tillite" 0.8%
Basic Granulite 1.4%
Metamorphics (not specified) 5%
Tuff 2%
Pyroclastics 2%
Basalt 47%
PS75/133-1
Diorite 9%
Granite 19%
not identified 1%
"Tillite" 7%
Basic Granulite 3%
Gneiss 2%
Metamorphics (not specified) 3%
Grt-Granite (Migmatite) 7%
Greenschist 8%
Rhyolite 2%
Hyaloclastite 5%
Pyroclastics 5%
Basalt 30%
PS75/130-2
Granite 49%
"Tillite" (0.2%)
Metamorphics (not specified) 1%
Greenschist 2%
Gneiss 3%
Felsic volcanics 0.3%
Pyroclastics 2%
Diorite 18%
Basalt 24%

Fig. 4

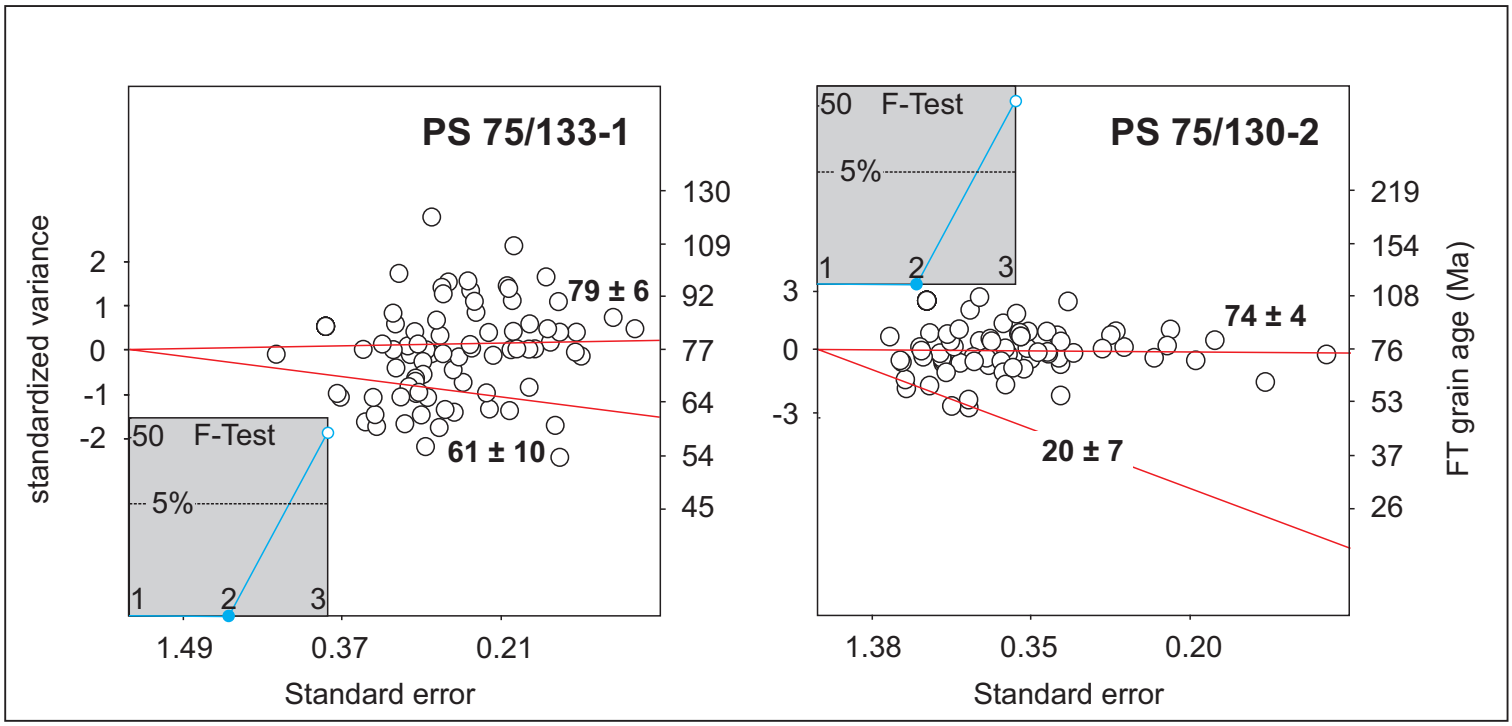
PS 75/133-1
PS 75/130-2
standardized variance
FT grain age (Ma)
Standard error
79 ± 6
61 ± 10
74 ± 4
20 ± 7
50 F-Test
5%
1
2
3
130
109
92
77
64
54
45
219
154
108
76
53
37
26
1.49
0.37
0.21
1.38
0.35
0.20

Fig. 5

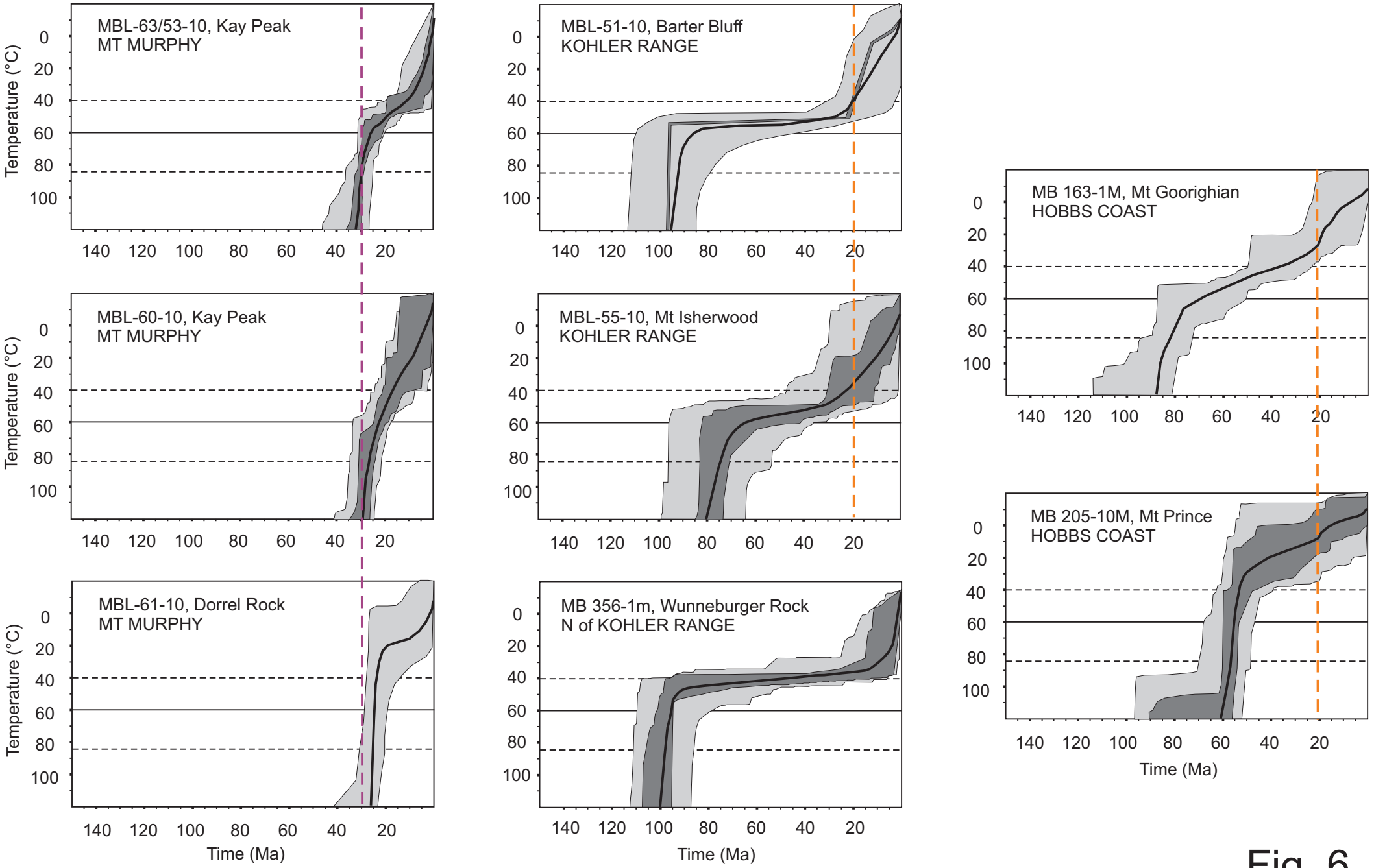
MBL-63/53-10, Kay Peak
MT MURPHY
MBL-51-10, Barter Bluff
KOHLER RANGE
MB 163-1M, Mt Goorighian
HOBBS COAST
MBL-60-10, Kay Peak
MT MURPHY
MBL-55-10, Mt Isherwood
KOHLER RANGE
MB 205-10M, Mt Prince
HOBBS COAST
MBL-61-10, Dorrel Rock
MT MURPHY
MB 356-1m, Wunneburger Rock
N of KOHLER RANGE
Temperature (°C)
0
20
40
60
80
100
140
120
100
80
60
40
20
Time (Ma)

Fig. 6

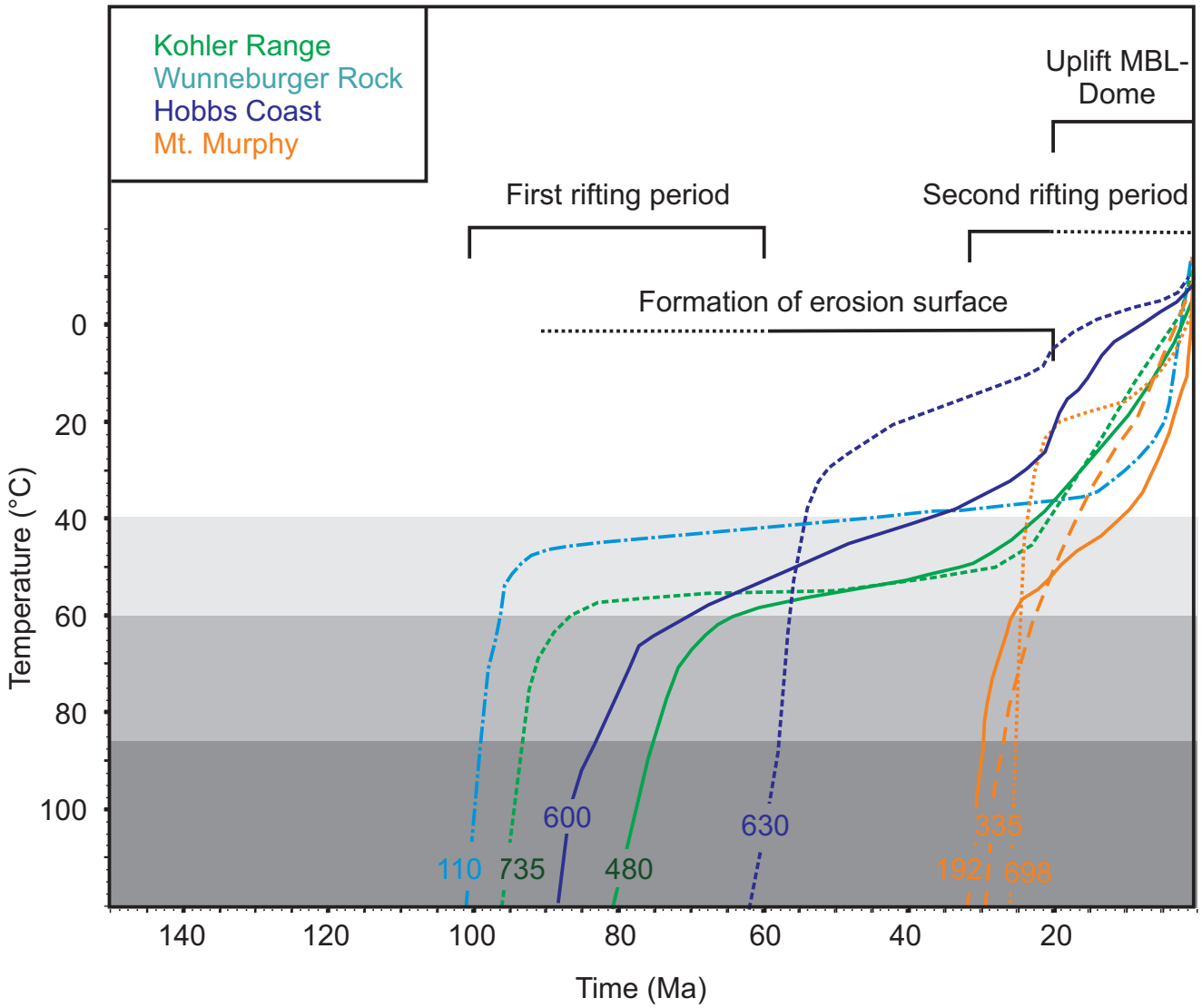
Kohler Range
Wunneburger Rock
Hobbs Coast
Mt. Murphy
Uplift MBL-Dome
First rifting period
Second rifting period
Formation of erosion surface
0
20
40
60
80
100
Temperature (°C)
140
120
100
80
60
40
20
Time (Ma)
110
735
480
600
630
335
192
698

Fig. 7

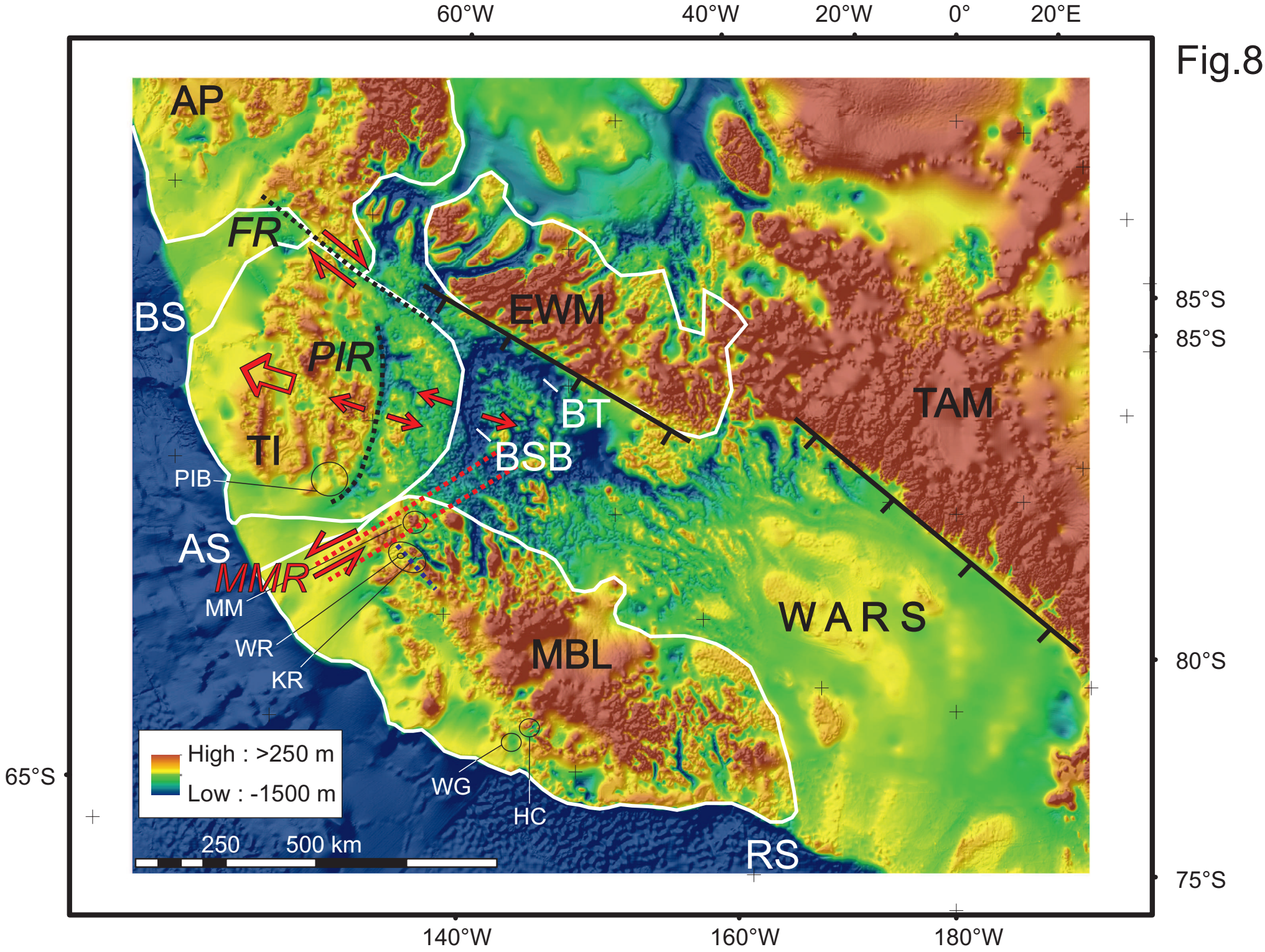
60°W
40°W
20°W
0°
20°E
85°S
85°S
80°S
75°S
65°S
140°W
160°W
180°W
AP
FR
BS
EWM
PIR
BT
TAM
TI
BSB
PIB
AS
MMR
MM
WR
KR
WARS
MBL
WG
HC
RS
High : >250 m
Low : -1500 m
250
500 km

Fig.8

Table 1: Results of AFT thermochronology on glaciomarine sediments / Wrigley Gulf

Code Elevation (m.a.s.l.)	n	ns	ρs (10^5 tracks/cm^2)	ni	ρi (10^5 tracks/cm^2)	nd	ρd (10^5 tracks/cm^2)	U (ppm)	central age (Ma)	P1	Frac (%)	P2	Frac (%)
PS75/130-2, -793	81	800	9.150	2888	33.033	23347	15.7	25	70 ± 4	20 ± 7	6	74 ± 4	94
PS75/133-1, -474	80	1867	21.208	6319	71.780	23347	15.6	54	74 ± 3	61 ± 10	25	79 ± 6	75

n - number of counted grains, ns / ρs - number and density of spontaneous tracks, ni / ρi - number and density of induced tracks
nd / ρd - number and density of tracks induced from dosimeter glass. $\zeta = 324 \pm 11$, calculated for dosimeter glass CN5
P1 / P2: age groups derived from data deconvolution, together with the relative amount of grains contained in each age group (Frac)

Table 2: Results of Fission Track thermochronology from nunataks of eastern Marie Byrd Land

Code	Location Elevation (m.a.s.l.)	n	ns	ρs (10^5 tracks/cm^2)	ni	ρi (10^5 tracks/cm^2)	nd	ρd (10^5 tracks/cm^2)	U (ppm)	central age (Ma)	P(X)^2 (%)	MTL (µm)	nMTL	SD (µm)	mean Dpar (µm)	SD (µm)
Apatite Fission Track																
MB 356-1m	Wunneburger Rock, 110	20	484	6.380	1090	14.37	3023	12.23	n.a.	93 ± 6	79	13.5	73	1.0	1.82	0.14
MB 402-1d	Mt. Wilbanks, 350	20	495	16.570	1422	47.61	2929	11.85	n.a.	71 ± 4	30	14.1	29	1.3	3.84	0.44
MB 412-1d	Mt. Meunier, 600	20	516	14.820	1513	43.46	2964	11.99	n.a.	70 ± 4	98	13.1	57	1.8	3.26	0.40
MBL-55-10	Mt. Isherwood, 480	19	108	4.183	407	15.762	28585	18.33	11	78 ± 9	99	13.4	88	1.7	1.91	0.19
MBL-51-10	Barter Bluff, 735	21	358	7.673	1155	24.754	28585	18.57	15	93 ± 6	83	13.5	104	1.3	1.98	0.21
MBL-60-10	Kay Peak, 335	21	189	7.586	2030	81.477	28585	19.43	48	29 ± 2	81	13.8	100	1.4	1.94	0.18
MBL-61-10	Dorrel Rock, 698	21	196	1.923	2111	20.711	28585	17.97	18	28 ± 2	100	14.5	45	0.7	1.98	0.17
MBL-63-10	Kay Peak, 192	21	116	3.747	1154	37.28	28585	19.19	23	31 ± 3	100	13.1	44	1.2	1.97	0.17
MB 163-1m	Mt. Goorhigian, 600	26	815	21.166	2639	68.537	23347	15.86	51	79 ± 5	14	13.2	113	1.5	1.81	0.11
MB 205-10m	Mt. Prince, 630	20	100	4.764	356	16.961	23347	15.86	13	72 ± 9	100	14.4	51	0.8	1.71	0.12
Zircon Fission Track																
MB 356-1m	Wunneburger Rock, 110	10	1931	125.16	1489	96.51	3032	12.59	n.a.	108 ± 4	32	n.a.	n.a.	n.a.	n.a.	n.a.
MB 412-1d	Mt. Meunier, 600	10	1489	163.65	1608	176.73	3032	13.01	n.a.	80 ± 3	100	n.a.	n.a.	n.a.	n.a.	n.a.

n - number of counted grains, ns / ρs - number and density of spontaneous tracks, ni / ρi - number and density of induced tracks
nd / ρd - number and density of tracks induced from dosimeter glass. MBL-samples: ζ = 324 ± 11, calculated for dosimeter glass CN5 . MB samples: ζ = 344 ± 5, calculated for dosimeter glass SRM 612.
MTL refers to non-c-axis corrected values

Table 3: Results of apatite (U-Th-Sm)/He thermochronology from nunataks of eastern Marie Byrd Land

Sample Code Locat. / Elevat. (r	raw age (Ma)	error (Ma)	corrected age (Ma)	error (Ma)	Ft weighted	^{4}He (ncc)	mass (µg)	Sm (ppm)	Th (ppm)	U (ppm)	eU (ppm)	r_{sphere} (µm)	mean age (Ma)	S.E. (Ma)	S.D. (Ma)
MBL-53-10															
Kay Peak, 192 m													**25**	**1.8**	**3.1**
#5	17.34	1.07	**24**	**3**	0.73	0.230	3.536	1.80	14.56	27.58	31.01	58			
#6	14.82	0.92	**22**	**3**	0.69	0.284	2.468	3.61	29.10	57.31	64.17	51			
#7	23.27	1.44	**28**	**3**	0.83	6.458	8.186	6.61	220.31	228.05	279.86	93			
#8	*28.02*	*1.75*	***49***	***6***	*0.57*	*0.527*	*0.432*	*6.99*	*227.32*	*305.47*	*358.93*	*33*			
MBL-60-10															
Kay Peak, 335 m													**23**	**1.5**	**2.5**
#1	17.67	1.10	**23**	**3**	0.76	0.332	4.772	30.91	19.40	28.60	33.32	66			
#2	13.89	0.86	**20**	**2**	0.70	0.054	2.364	26.11	26.05	7.22	13.48	52			
#4	16.50	1.02	**25**	**3**	0.65	0.131	2.151	11.91	13.78	27.19	30.49	46			
MBL-61-10															
Dorrel Rock, 698 m													**18**	**2.0**	**n.a.**
#1	14.28	0.89	**18**	**2**	0.80	0.070	7.789	8.69	9.08	2.98	5.16	82			
#3	*33.75*	*2.09*	***34***	***2***	*1.00*	*0.041*	*1.209*	*18.10*	*19.16*	*3.61*	*8.21*	*46*			
#4	*37.67*	*2.34*	***38***	***2***	*1.00*	*0.067*	*1.572*	*19.91*	*16.63*	*5.24*	*9.25*	*52*			
MB 356-1m															
Wunneburger Rock, 110 m													**67**	**8.8**	**4.4**
#1	52.72	3.27	**69**	**8**	0.76	1.036	4.715	59.31	52.21	21.52	34.10	66			
#2	51.39	3.19	**79**	**9**	0.65	0.312	1.634	67.27	66.66	14.31	30.33	45			
#3	49.24	3.05	**60**	**7**	0.82	1.604	9.997	49.80	37.53	17.58	26.66	86			
#4	40.44	2.51	**61**	**7**	0.66	0.252	1.917	54.92	44.88	15.75	26.59	47			
MBL-55-10															
Mt. Isherwood, 480 m													**54**	**1.5**	**0.9**

#1	39.20	2.43	**54**	**6**	0.73	0.141	2.066	12.93	19.36	9.68	14.30	60		
#2	37.26	2.31	**56**	**7**	0.66	0.140	2.209	17.04	18.56	9.50	13.95	48		
#3	35.34	2.19	**53**	**6**	0.67	0.122	2.182	12.03	16.04	9.17	13.00	49		
MBL-57-10														
Morrison Bluff, 488 m														
#1	*49.28*	*3.06*	***77***	***9***	*0.64*	*0.985*	*1.665*	*16.07*	*121.74*	*70.37*	*99.06*	*72*		
MBL-51-10														
Barter Bluff, 735 m													**42**	**7.2**	**4.2**
#1	28.13	1.74	**36**	**4**	0.78	0.478	7.191	43.85	31.60	11.68	19.34	74		
#2	33.18	2.06	**50**	**6**	0.66	0.123	1.656	29.08	36.24	9.66	18.33	47		
#4	29.85	1.85	**40**	**6**	0.76	0.305	4.524	41.17	37.00	9.55	18.46	65		
MB 204-3/4m														
Mt. Goorighian, 360 m														
#1	*82.68*	*5.13*	***128***	***15***	*0.65*	*1.535*	*1.800*	*66.35*	*187.91*	*39.86*	*84.37*	*47*		
#2	*39.20*	*2.43*	***71***	***8***	*0.56*	*0.127*	*0.527*	*61.24*	*17.19*	*46.18*	*50.54*	*36*		
MB 163-1m														
Mt. Goorighian, 600 m													**63**	**1.4**	**1.0**
#2	48.26	2.99	**64**	**7**	0.76	1.559	5.573	49.75	16.81	43.43	47.64	67		
#3	48.55	3.01	**62**	**7**	0.78	1.157	3.566	72.78	23.64	48.95	54.89	72		
MB 205-10m														
Mt. Prince, 630 m													**56**	**1.0**	**1.4**
#1	40.19	2.49	**57**	**7**	0.71	0.233	3.627	72.07	19.46	7.99	12.95	57		
#2	39.77	2.47	**55**	**6**	0.73	0.262	2.542	102.09	32.55	12.85	21.04	59		

Ft - a-ejection correction after Farley et al. (1996); eU - effective U-concentration

r_{sphere} - equivalent sphere radius of measured crystal, S.E. - standard error, S.D. - standard deviation

All aliquots refer to single-grain measurements

Figures in italics: excluded from thermal history modelling

Table 1: Lithologies and crystallization ages of non-volcanic rocks in eastern Marie Byrd Land

Nunatak	Area	Lithology	Age (Ma)	Reference
Bailey Nunatak	Western Hobbs Coast	Lithic Graywacke	n.a.	Brand, 1979
Bennett Bluff	Western Hobbs Coast	Meta-igneous Rocks	n.a.	Brand, 1979
Cape Burks	Western Hobbs Coast	Olivin Gabbro	n.a.	Lopatin & Orlenko, 1974
Dorrel Rock	Mt Murphy	Gabbro	34.2 ± 0.2	Rocchi et al., 2006
Early Bluff	Kohler Range	Pink Granite	103.4 ± 0.3	Mukasa & Dalziel, 2000
Holmes Bluff	Demas Range	Megacrystic Granite	113 ± 2	Mukasa & Dalziel, 2000
Jeffrey Head	Bear Peninsula	Granodiorite, Monzogranite, Gabbro-Diorite	312 ± 10	Pankhurst et al., 1998
Kay Peak	Mt Murphy	Biotite-Muscovite Syenogranite	229 ± 10	Pankhurst et al., 1998
Kay Peak	Mt Murphy	Microgranite	262 ± 5	Pankhurst et al., 1998
Kay Peak	Mt Murphy	Microgranite	353 ± 2	Mukasa & Dalziel, 2000
Kay Peak	Mt Murphy	Ortho-Gneiss	505 ± 5	Pankhurst et al., 1998
Kinsey Ridge	Western Hobbs Coast	Hornblende-Biotite Monzogranite	239 ± 4	Pankhurst et al., 1998
Klimov Bluff	Kohler Range	Granodiorite	113 ± 6	Mukasa & Dalziel, 2000
Lewis Bluff	Western Hobbs Coast	Granite	n.a.	Brand, 1979
Mt Goorhigian	Demas Range	Leucocratic Granitic Gneiss	128 ± 2	Mukasa & Dalziel, 2000
Mt Goorhigian	Demas Range	Megacrystic Granite	127 ± 1	Mukasa & Dalziel, 2000
Mt Goorhigian	Demas Range	Garnet-bearing Granite	118 ± 5	Mukasa & Dalziel, 2000
Mt Hartkopf	Western Hobbs Coast	Granite	n.a.	Brand, 1979
Mt Hartkopf	Western Hobbs Coast	Tremolith-Epidote-Wollastonite Schist	n.a.	Brand, 1979
Mt Isherwood	Kohler Range	Biotite-Hornblende Granodiorite	243 ± 29	Mukasa & Dalziel, 2000
Mt Isherwood	Kohler Range	Biotite Monzogranite	276 ± 2	Pankhurst et al., 1998
Mt Langway	Western Hobbs Coast	Syenite	102 ± 1	Mukasa & Dalziel, 2000
Mt Langway	Western Hobbs Coast	Alkali Granite	98.9 ± 0.3	Mukasa & Dalziel, 2000
Mt McCoy	Western Hobbs Coast	Granodiorite	320 ± 3	Mukasa & Dalziel, 2000
Mt Meusnier	Kohler Range	Quartz-Diorite to Granodiorite	113 ± 2	Mukasa & Dalziel, 2000
Mt Pearson	Western Hobbs Coast	Lithic Graywacke	n.a.	Brand, 1979
Mt Prince	Western Hobbs Coast	Calc-alkaline Granite	110 ± 1	Mukasa & Dalziel, 2000
Mt Prince	Western Hobbs Coast	Mafic and Intermediate Dykes	101 ± 1	Mukasa & Dalziel, 2000
Mt Steinfeld	Western Hobbs Coast	Granodiorite	116 ± 1	Mukasa & Dalziel, 2000

Mt Strange	Kohler Range	Bt-Hbl-Diorite, Bt-Monzogranite, Grt-Ms Aplite	276 ± 2	Pankhurst et al., 1998
Mt Vance	Western Hobbs Coast	Syenite	102 ± 1	Mukasa & Dalziel, 2000
Mt Wilbanks	Kohler Range	Quartz-Diorite	283 ± 0.5	Mukasa & Dalziel, 2000
Navarette Peak	Mt Petras, McCuddin Range	Qtz-Pl-Ms-Chl-Grt Schist	340-380	Brand, 1979
Nickols Rock	Western Hobbs Coast	Feldspatic Greywacke	n.a.	Brand, 1979
Patton Bluff	South of Demas Range	Granitoid	Cretaceous	Pankhurst et al., 1998
Patton Bluff	South of Demas Range	Paragneiss enclave	~330 Ma (Protolith)	Pankhurst et al., 1998
Peacock Peak	Western Hobbs Coast	Quartz-Hornblende-Tremolith Schist	n.a.	Brand, 1979
Peden Cliffs	Western Hobbs Coast	Quartz Syenite	99.3 ± 0.7, 98.4 ± 0.8	Mukasa & Dalziel, 2000
Rogers Spur	Bear Peninsula	Andesitic Breccia	150	Lopatin et al., 1974
Shepard Island	Hobbs Coast	Quartzite	n.a.	Lopatin & Orlenko, 1974
Southeast Spur	Mt Petras, McCuddin Range	Granodiorite	111 ± 5	Mukasa & Dalziel, 2000
Wallace Rock	Mt Petras, McCuddin Range	Quartz-Biotite-Muscovite Schist	n.a.	Brand, 1979
Wilkins Nunatak	Western Hobbs Coast	Syenite	101.8 ± 0.3	Mukasa & Dalziel, 2000
Wilkins Nunatak	Western Hobbs Coast	Arkose-Conglomerate, Quartzite	n.a.	Brand, 1979
Wunneburger Rock	Martin Peninsula	Diorite	129 ± 9	Mukasa & Dalziel, 2000

Table 2: Samples analysed for this study

Sample Code	Location	Lithology	Latitude	Longitude	Elevation
Hobbs Coast					
MB 163-1m	Mt Goorhigian	megacrystic granite	S 75° 03.7`	W 133° 43.2`	600 m
MB 204-4m	Mt Goorhigian	foliated diorite	S 75° 03`	W 133° 48`	360 m
MB-204-3m	Mt Goorhigian	leucocratic gneiss	S 75° 03`	W 133° 48`	360 m
MB 205-10m	Mt Prince	granite	S 74° 58`	W 134° 10`	630 m
Kohler Range					
MBL-51-10	Barter Bluff	granite	S 75° 09.59`	W 113° 58.70`	735 m
MBL-57-10	Morrison Bluff	gabbro	S 75° 05.10`	W 114° 19.50`	488 m
MBL-55-10	Mt Isherwood	coarse white granite	S 74° 58.99`	W 113° 41.63`	480 m
MB 402-1D	Mt Wilbanks	microgranite	S 75° 00`	W 112° 53`	350 m
MB 412-1D	Mt Meunier	quartz diorite	S 74° 57`	W 113° 19`	600 m
MB 356-1m	Wunneburger Rock	diorite	S 74° 42.4`	W 113° 11`	110 m
Mt. Murphy					
MBL-63-10	Kay Peak	leucogranite	S 75° 13.05`	W 110° 57.80`	192 m
MBL-53-10	Kay Peak	amphibolite	S 75° 13.05`	W 110° 57.80`	192 m
MBL-60-10	Kay Peak	migmatitic gneiss	S 75° 13.23`	W 110° 57.58`	335 m
MBL-61-10	Dorrel Rock	gabbro	S 75° 26.67`	W 111° 22.06`	698 m
Wrigley Gulf					
PS 75/130-2	offshore Berry Glacier	glaciomarine sediment	S 74° 26.73`	W 134° 09.16`	-793 m
PS 75/132-1	offshore Berry Glacier	glaciomarine sediment	S 74° 22.03`	W 134° 22.95`	-750 m
PS 75/133-1	offshore Berry Glacier	glaciomarine sediment	S 74° 20.64`	W 133° 04.68`	- 474 m

A

B

C

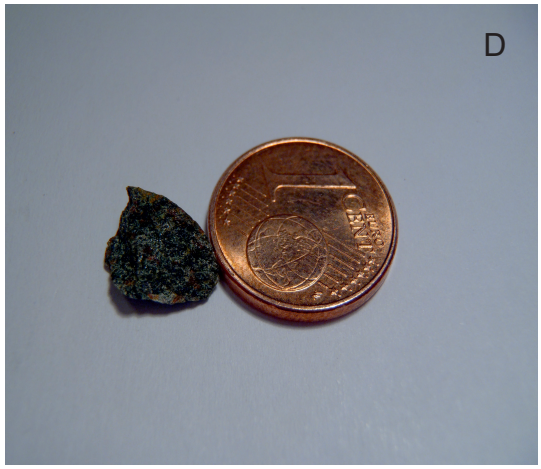

D

E

F

G

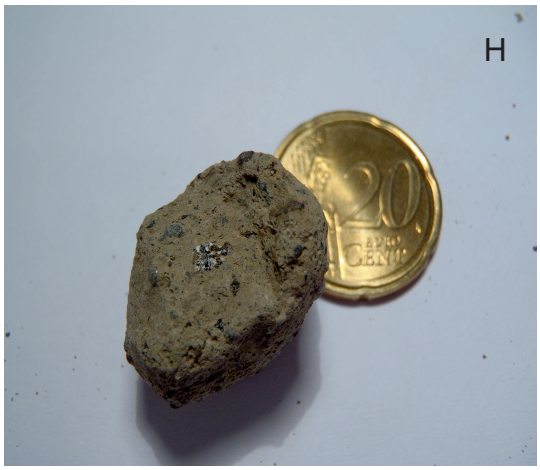

H

Fig. A1

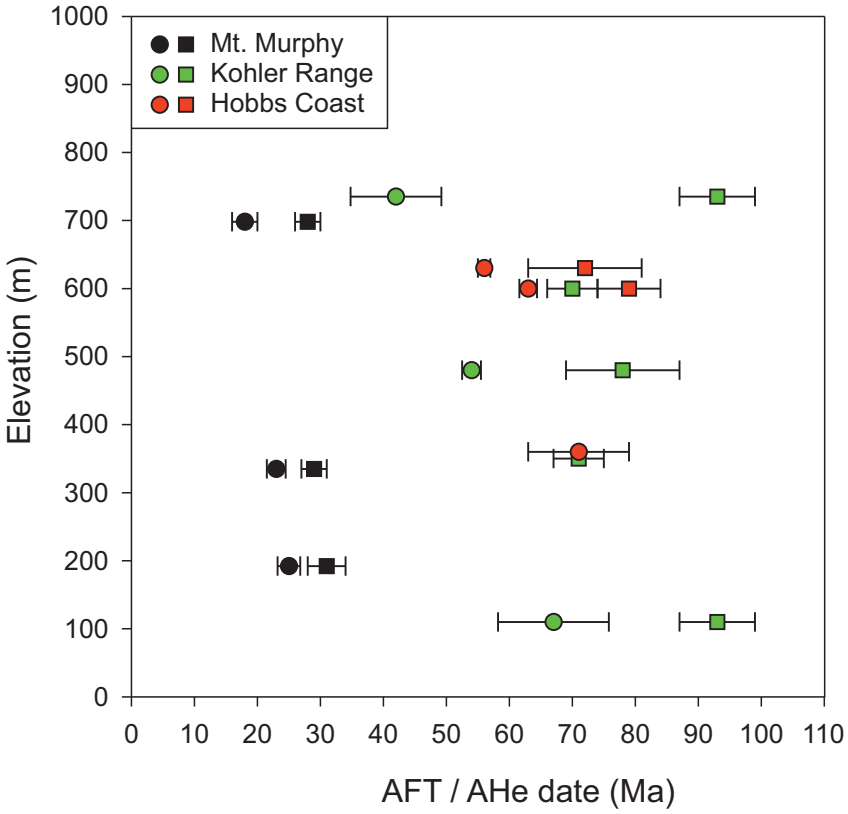
Mt. Murphy
Kohler Range
Hobbs Coast
Elevation (m)
1000
900
800
700
600
500
400
300
200
100
0
0
10
20
30
40
50
60
70
80
90
100
110
AFT / AHe date (Ma)

Fig. A2